ELSEVIER

Journal of Structural Geology 28 (2006) 1785–1807

JOURNAL OF STRUCTURAL GEOLOGY

www.elsevier.com/locate/jsg

Relief and shortening in detachment folds

Ramon Gonzalez-Mieres*, John Suppe

Department of Geosciences, Princeton University, Princeton, New Jersey 08544-1003, USA

Received 6 January 2006; received in revised form 10 July 2006; accepted 11 July 2006
Available online 12 September 2006

Abstract

We present new *thickness-relief methods* for determining shortening $S(z)$, mean shortening $\overline{S}(z)$ and curvimetric shortening $S_c(z)$ as a function of height in well-imaged structures. Thickness-relief measurements allow us to constrain the fractions of the deformation that are layer-parallel pure shear, simple shear, and flexural, and to measure the excess area A_e of fold cores caused, for example, by flow of evaporites. The key measurements are made in the thickness domain, which allows for more certain determination of regional stratigraphic gradients, which is required for reliable separation of structural relief from primary stratigraphic thickness variations. We apply these methods to a diverse set of active detachment folds from the fronts of the Nankai trough Japan, Cascadia accretionary wedge Oregon, southern Tianshan China and Agbami anticline deep-water Niger delta. Three of these folds can be approximated by pure-shear detachment fold models because more than 95% of the shortening is by layer-parallel heterogeneous pure shear plus horizontal compaction. For this reason curvimetric shortening is one to two orders of magnitude less than total shortening. In contrast, Agbami anticline shows layer-parallel stretching above the excess area of the fold core. In all examples the layer-parallel simple-shear component is negligible or absent.

Keywords: Detachment folding; Structural relief; Thickness relief; Bed-length shortening; Depth to detachment; Pure shear; Simple shear; Tectonic compaction; Nankai trough; Cascadia subduction zone; Yakeng anticline Tianshan China; Agbami anticline Niger delta

1. Introduction

Detachment folding seems conceptually very simple from a mass-balance perspective, with all the shortening consumed in folding above a weak detachment layer (Laubscher, 1961, 1965; Jamison, 1987; Groshong and Epard, 1994; Poblet and McClay, 1996). Classically, by conservation of area within a closed cross-sectional system (Fig. 1), the area A_s displaced into the fold by shortening of layers below a given stratigraphic horizon has been considered equal to the area of structural relief A_{sr} that is displaced upward in folding of the same horizon above its undeformed regional level (Chamberlain, 1910; Bucher, 1933; Goguel, 1962; Laubscher, 1965). This area of shortening A_s would then be equal to the mean shortening $\overline{S}$ times the undeformed height H_d of the horizon above the base of the detachment layer

$$A_{sr} = A_s = \overline{S} H_d \tag{1}$$

The mean shortening can be obtained simply by dividing the measured area of structural relief by the height above the detachment

$$\overline{S} = A_{sr}/H_d \tag{2}$$

which has been called *planimetric shortening* by Laubscher (1961, 1966) and in general may vary as a function of stratigraphic height z, so we write $\overline{S}(z)$, as shown in Figs. 1 and 2.

These classic relationships between structural relief and shortening have become more interesting in recent years because of improved imaging, including both seismic imaging of large-scale structures and surveying of folds exposed at the surface using photogrammetric, geodetic, laser and other

* Corresponding author. Tel.: +1 609 2581515; fax: +1 609 2581671.
E-mail address: ragonzal@princeton.edu (R. Gonzalez-Mieres).

0191-8141/$ - see front matter © 2006 Elsevier Ltd. All rights reserved.
doi:10.1016/j.jsg.2006.07.001

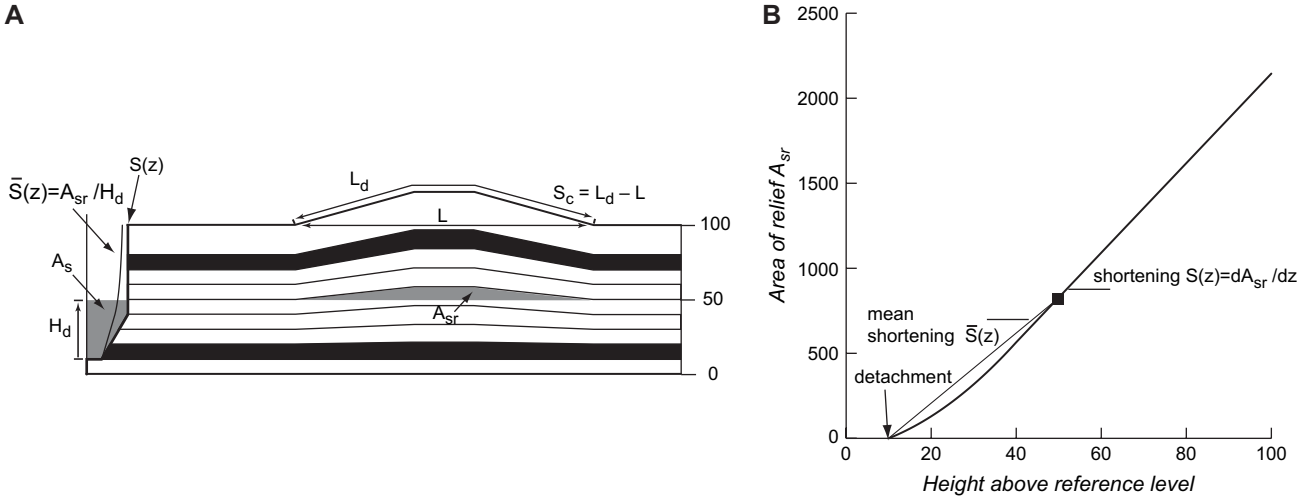

Fig. 1. (A) A simple detachment fold model with variable shortening as a function of height z. Three contrasting measures of shortening are shown: bed-by-bed shortening $S(z)$, mean shortening $\bar{S}(z)$, and curvimetric or bed-length shortening S_c. The quantities that we need to observe as a function of height to determine the shortening are: the area of structural relief A_{sr} which is the area of deflection of a deformed horizon from its undeformed elevation or *regional*; the undeformed height H_d of the horizon above a detachment; the deformed length of a horizon L_d and the straight-line length L measured along the regional. The area of structural relief A_{sr} in this model is equal to the area of shortening A_s, but we also consider cases in which they differ for structurally interesting reasons. (B) Following Epard and Groshong (1993), measurements of area of relief as a function of height can be plotted such that the local slope of the data gives the shortening $S(z)$. Note that the mean shortening above a detachment $\bar{S}(z)$ will be in general different from the shortening $S(z)$.

techniques (Poblet and Hardy, 1995; Erslev and Mayborn, 1997; Rico, 1999; Atkinson and Wallace, 2003). Essentially complete imaging allows us to measure the area of structural relief on many imaged stratigraphic horizons, offering the possibility of fine-scale determination of shortening as a function of stratigraphic level. In particular, Epard and Groshong (1993) showed that if we plot the measured areas of structural relief for a number of stratigraphic horizons as a function of height above the detachment or any reference level, the slope of the data is the shortening (Fig. 1B). With increasing shortening there is an increasing slope to the height–area plot. These relationships are not confined to detachment folds and have been applied to both compressional and extensional structures (Epard and Groshong, 1993, 1995; Groshong and Epard, 1994, 1996; Pashin et al., 1995; Adam et al., 2004; Higuera-Díaz et al., 2005; Hubert-Ferrari et al., 2005).

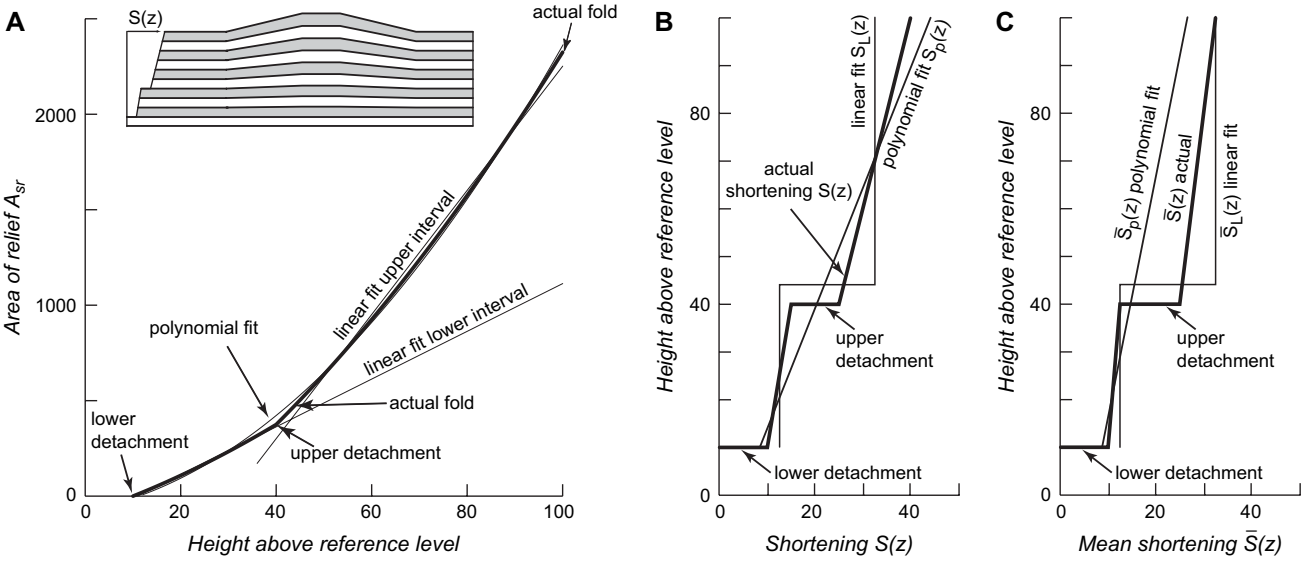

Fig. 2. (A) Area relief graph of a more complex detachment fold model containing two detachments and layer-parallel simple shear. (B) Shortening as a function of height. (C) Mean shortening as a function of height. These graphs illustrate the challenges of recovering the shortening $S(z)$ as a function of height from measurements of area of structural relief A_{sr}. It is possible to obtain improved estimates of shortening $S(z)$ by simultaneously considering the mean shortening $\bar{S}(z)$ and the shortening obtained from linear $S_L(z)$, polynomial $S_p(z)$ and other approximations to the data. A key element in the analysis is computing the mean shortening predicted from the linear $\bar{S}_L(z)$, polynomial $\bar{S}_p(z)$ and other approximations and comparing them with the observed mean shortening $\bar{S}(z)$. These techniques work well in our four case studies.

Nevertheless, determining the shortening from area of structural relief is not entirely straightforward for several reasons that are addressed in this paper:

[1] Stratigraphic and structural complexities in many cases make it difficult or impossible to determine accurately the undeformed regional level of a stratigraphic horizon, which is required for determining both area of structural relief and height. The problem is that the regional level may have a complex shape that is not obvious by inspection in the present deformed state, in contrast with the simple picture in Fig. 1. Hubert-Ferrari et al. (2005) suggested that this problem may be overcome in many cases by making measurements in the *thickness domain* rather than in the *depth domain* of the present deformed cross-section, allowing a more straightforward determination of the undeformed regional level and hence the area of relief. We call this the *thickness-relief method*, which we outline in substantially more detail than was possible in the initial presentation by Hubert-Ferrari et al. (2005). Our examples apply this method.

[2] In general shortening may vary as a function of stratigraphic height, hence we write $S(z)$. Therefore the area of structural relief of a horizon is the shortening integrated over the height above the detachment

$$A_{sr}(z) = \overline{S}(z)H_d = \int_0^{H_d} S(z)\mathrm{d}z \tag{3}$$

but the shortening of a horizon is the vertical gradient in the area of structural relief

$$S(z) = \mathrm{d}A_{sr}/\mathrm{d}z \tag{4}$$

Thus it is not surprising that, whereas it is relatively easy to determine mean shortening $\overline{S}(z) = A_{sr}(z)/H_d$, it is substantially more difficult to determine the layer-by-layer shortening $S(z)$ from measurements of structural relief because of errors in the data. Furthermore $S(z)$ may not always be smoothly varying or everywhere continuous because of stratigraphic complexities in the deformation, such as multiple detachments or layer-parallel shear (Figs. 1 and 2). For these reasons our ability to measure $S(z)$ is practically limited by our ability to measure $A_{sr}(z)$, as we shall see from our examples.

[3] The assumption of conservation of area in a 2D closed system does not always hold for structurally significant reasons. For example, conservation of area is violated in the case of horizontal tectonic compaction, which appears to be quantitatively important in some low-amplitude detachment folds (Henry et al., 2003), including several of our examples. More importantly there is sometimes quite substantial layer-parallel flow of salt or shale within the basal detachment layer or other stratigraphic intervals, such that neither area nor height is locally conserved (Wiltschko and Chapple, 1977; Homza and Wallace, 1995, 1997). Under these circumstances the measured area of structural relief must have a more complex relationship to mean shortening. As a simple example, if there is an increase in area A_e of the core of a detachment fold as a result of flow of material within the basal layer, Eq. (2) could become

$$\overline{S} = (A_{sr} - A_e)/H_d \tag{5}$$

In several of our examples these effects are quantitatively substantial.

Our discussion so far has been focused on determining shortening from measurements of area of structural relief. Traditionally shortening has also been estimated from the difference between the deformed bed length L_d and the length of the bed along the regional L between the same end points (Fig. 1), based on the assumption of conservation of bed length ($L_d = L_o$)

$$S_c = (L_d - L) \tag{6}$$

which has been called the *curvimetric shortening* by Laubscher (1961). However, in some cases bed length is not conserved $L_d \neq L_o$, in which case the measured curvimetric shortening S_c is not equal to the shortening S because of shortening (or stretching) due to strain S_ε

$$S = S_c + S_\varepsilon \tag{7}$$

The curvimetric shortening can be one or even two orders of magnitude different from the actual shortening, as we shall see in the examples. In the limiting case of deflection of the overburden above a flowing basal evaporite layer there may be no tectonic shortening at all, in which case the measured "curvimetric shortening" will be the increase in bed length S_ε due to stretching of the overburden. Thus, we should think of the curvimetric shortening as the component of apparent shortening associated with deflection or flexure of the layer from the regional. By simultaneously measuring S_c, $S(z)$ and $\overline{S}$ it may be possible to identify deflectional (flexural), pure shear (S_ε) and simple-shear components of the total shortening.

The combined measurement of curvimetric shortening S_c and area of structural relief A_{sr} has long been used to estimate the depth to detachment H_d, starting with the well known but quantitatively unsuccessful attempt of Chamberlain (1910, 1919) to determine the thickness of the deformed crustal shell of the Appalachians and Rocky Mountains, based on inserting S_c into Eq. (1)

$$H_d = A_s/\overline{S} \approx A_{sr}/S_c \tag{8}$$

It has been widely noted that this depth to detachment calculation in many cases overestimates the depth, including the cases of Chamberlain (Bucher, 1933; Wiltschko and Chapple, 1977; Mitra and Namson, 1989; Epard and Groshong, 1993; Homza and Wallace, 1995; Bulnes and Poblet, 1999). The two most common reasons for this failure are: [1] Eq. (8) overestimates the depth because curvimetric shortening S_c is commonly much less than the mean shortening $\overline{S}$. [2] In cases in which there is substantial flow within a basal detachment layer

the measured area of structural relief A_{sr} is substantially larger than the area of shortening A_s, as illustrated in Eq. (5), therefore Eq. (8) overestimates the depth to detachment.

In the following sections we first present a summary of the *thickness-relief method*, which gives us improved measurements of A_{sr}. Then we apply these methods and concepts to estimate the various components of shortening as a function of height in pregrowth strata of four detachment folds in the active thrust belts of the Nankai trough offshore Japan, Cascadia offshore Oregon, southern Tianshan China, and Niger delta. In a separate paper we address the issue of determining the history of deformation based on measurements of thickness relief in growth strata, applied to the same four examples (Gonzalez-Mieres and Suppe, submitted for publication).

2. The thickness-relief method

The deformed shape of any set of horizons is the final result of a convolution of stratigraphic and structural complexities that in practice make it difficult or impossible to reliably identify the regional stratigraphic level in the classical way by inspection (Fig. 3a). The expected shape of the regional level is not entirely obvious in the present deformed state because of stratigraphic thickness variations, deformation of the footwall of the structure in question, interference with adjacent independent folds, and lateral flow of mobile stratigraphic intervals such as evaporites (Hubert-Ferrari et al., 2005). Thus the key issue is determining what part of the shape is structural and what part is stratigraphic for each mapped horizon, which requires human judgment. Hubert-Ferrari et al. (2005) proposed that this distinction is in many cases much more easily made in the *thickness domain* than in the *depth domain* of a normal structural cross-section. The thickness domain is simply the structural cross-section or seismic line flattened to a specific mapped stratigraphic horizon. The flattening in this paper is done using vertical simple shear such that area and vertical thickness are conserved. In this flattened state it is typically possible to distinguish regional thickness gradients from structure (Fig. 3b), especially if the section is much longer than the scale of the structure. These measurements of area of relief and thickness are thus local differences in relief and height between nearby horizons. The measurements are independent of any assumptions or knowledge of locations of detachment horizons, or even their existence.

We adopt a notation (see Appendix A) that indicates a measured area of thickness relief of a horizon n relative to a *flattening level* f as a difference in relief $\Delta A_{f,n}$ between the two horizons, with an associated difference in height $\Delta H_{f,n}$. For example $\Delta A_{3,5}$ is the thickness relief of horizon 5 relative to a flattening level 3 (Fig. 3b). In compression $\Delta A_{f,n}$ is positive for horizons above the flattening horizon $(n > f)$ and negative below in the case of pregrowth strata (Fig. 3b).

It is best to use a well-imaged continuous horizon as a flattening horizon, with some attention to the stratigraphic architecture of the basin. Typically we use several flattening horizons for a single structure. An example of how we choose appropriate flattening horizons is given below for the Nankai

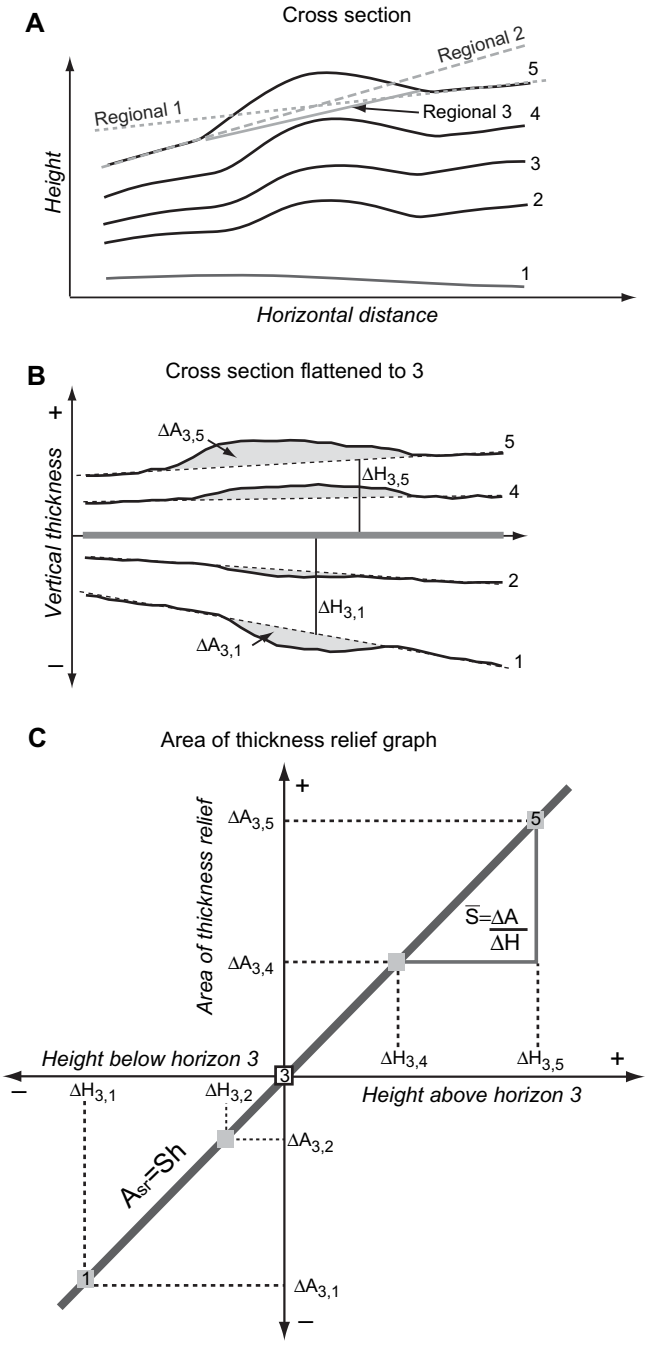

Fig. 3. The thickness-relief method. (A) The choice of the regional undeformed elevation of a horizon, such as 5, is commonly ambiguous in depth cross-sections in contrast with the simple model of Fig. 1. The ambiguity arises because the present shape of a horizon is a convolution of primary stratigraphic geometry, the structure of interest, other deformation below the structure, and flow of weak layers. (B) As suggested by Hubert-Ferrari et al. (2005) these ambiguities in many cases disappear if the structure is flattened to a suitable stratigraphic horizon, in this case horizon 3. This flattening is done by vertical simple shear such that area and vertical thickness is conserved. In the flattened domain the regional can be relatively easily identified in many cases, such that the differences in relief and height between nearby horizons can be measured unambiguously, for example $\Delta A_{3,5}$ and $\Delta H_{3,5}$. These measurements of thickness relief and height can be used to determine shortening as shown in (C) and discussed in the text and Appendix A.

trough. We then combine these independent sets of thickness-relief measurements $\langle \Delta A_{f,n}, \Delta H_{f,n} \rangle$ for each flattening horizon, using techniques described in Appendix A, to obtain a stratigraphically more comprehensive set of areas of structural relief and heights $\langle \Delta A_{r,n}, \Delta H_{r,n} \rangle$ relative to some datum or reference horizon of interest r, such as a detachment. Typically the final results $\langle A_{r,n}, H_{r,n} \rangle$ can be considered areas of structural relief and heights above the detachment in the classical sense.

The shortening $S_{m,n}$ for some local interval between horizons m and n can be immediately calculated from the thickness-relief measurements

$$S_{m,n} = \Delta A_{m,n} / \Delta H_{m,n} \tag{9}$$

independent of any detachment levels (Fig. 3c). However, the data may have significant errors or scatter leading to local shortening estimates of questionable accuracy. Therefore it may be useful to smooth the data or fit the data over a significant stratigraphic interval to some appropriate function, which then is differentiated to obtain $S(z)$.

However, even with perfect data, indiscriminate fitting of functions to the data can yield quite misleading results for several reasons, as illustrated in Fig. 2 and in our geologic examples. [1] Typical data can be fit reasonably well by several different functions that have very different derivatives, yielding very different estimates of $S(z)$. However, the quality of these different functional fits can be discriminated, if the detachment horizons are known, because they yield very different predictions of mean shortening as a function of height $\overline{S}(z)$, which can be easily compared with data as illustrated in Fig. 2. In our examples we were able to arrive at stronger claims about shortening as a function of height by simultaneously considering both $S(z)$ and $\overline{S}(z)$. [2] If more than one detachment horizon exists within a structure then $S(z)$ is discontinuous and the data on the two sides of the detachment must be analyzed independently. If a detachment exists within a structure and is not recognized in the analysis, quite erroneous results can be obtained, as illustrated in Fig. 2. [3] The behavior of growth strata is more complex because the vertical gradient in the area of relief is no longer simply equal to the shortening but is also a function of the sedimentation rate relative to the deformation rate (Gonzalez-Mieres and Suppe, submitted for publication). Therefore a direct application of these techniques to growth strata will yield erroneous results.

We have just considered some sources of erroneous shortening estimates that can arise from inappropriate choices at the stage of analyzing the relief data, $\langle \Delta A_{f,n}, \Delta H_{f,n} \rangle$ and $\langle A_{r,n}, H_{r,n} \rangle$. In addition these relief data contain errors that propagate from a variety of sources, including seismic imaging, depth conversion, horizon mapping and choice of regional stratigraphic gradient. We do not have sufficient constraints for our specific examples to make a useful analysis of specific sources of error and how they propagate to the final data. Therefore, we use simple linear regression to estimate the expected magnitude of the error for individual data pairs of $\Delta A_{f,n}, \Delta H_{f,n}$ (Weimer, 1987; Freund, 1997). This is justified to some extent in retrospect for our specific examples because we conclude at the end of the analysis that a linear regression is appropriate because these examples show a relatively constant shortening as a function of height (in contrast with the model folds of Figs. 1 and 2). However, the actual data errors could be substantially smaller than these formal error estimates from linear regression if shortening is more heterogeneous at a finer scale, which is a possibility we discuss later.

3. Computation of curvimetric shortening

Conservation of bed length has been traditionally assumed for many compressive structures in the upper crust. However, as proposed by Groshong and Epard (1994) layer-parallel shortening (heterogeneous pure shear) may play a central role in some detachment folding. We can use the difference between the shortening based on area of relief $S(z)$ and curvimetric or bed-length shortening S_c in natural examples to directly evaluate the role of layer-parallel pure shear shortening S_ε in detachment folds (Eq. (7)). The same low-level thickness-relief data may be used for both analyses.

Measurement of curvimetric shortening S_c, based on Eq. (6), requires knowledge of the undeformed regional position of the bed as well as its deformed shape (Fig. 1). In the thickness-relief analysis we determine the location of the regional stratigraphic gradient in the flattened state. However, we cannot use this regional gradient directly for computing line-length shortening because line length is not conserved in the transformation to the flattened state (thickness domain). Therefore we have to transform the regional stratigraphic gradient that is interpreted in the flattened state back into the undeformed state (the depth domain). The method is similar to that used in transforming measurements of thickness relief into areas of structural relief and is explained in Appendix B.

4. Relief and shortening of natural examples

There has been relatively little study of well-imaged detachment folds from a quantitative perspective (Rowan et al., 1993; Rowan, 1997; Masaferro et al., 1999). In particular there have been only a few analyses of shortening on a bed-by-bed basis (Epard and Groshong, 1993, 1995; Groshong, 1994, 1996; Pashin et al., 1995; Hubert-Ferrari et al., 2005). Here we apply a combination of thickness-relief and curvimetric shortening methods to determine the relationships between relief, shortening and bed length as a function of height in four detachment folds near the front of four active thrust belts: Nankai trough offshore Japan, Cascadia offshore Oregon, Yakeng anticline in the southern Tianshan China and Agbami anticline in the deep-water Niger delta. In this paper we report only the results for pregrowth strata. The analysis of growth strata is given by Gonzalez-Mieres and Suppe (submitted for publication).

4.1. Nankai detachment fold, offshore Japan

4.1.1. Geological framework

We analyze the active frontal detachment fold at the toe of the Nankai trough accretionary wedge, which lies along the

Cape Muroto transect (Fig. 4) offshore of southwest Japan (Le Pichon et al., 1987; Taira et al., 1992; Shipboard-Scientific-Party, 2001a). The convergence rate between the Philippine Sea and Eurasian plates in this region has been generally estimated at 2–4 cm/yr for the last 6 Ma (Seno, 1977; Karig and Angevine, 1986), however, recent GPS and stratigraphic studies propose a higher rate of 5–6 cm/yr for the last 3 Ma (Miyazaki and Heki, 2001; Moore et al., 2001b; Shipboard-Scientific-Party, 2001b).

This detachment fold (Fig. 4) is the principal structure within the ~5 km wide zone of distributed deformation ahead of the frontal thrust ramp called the *protothrust zone* (Moore et al., 1990). This zone shows structural thickening, seaward tilting and landward-increasing seismic velocities in the trench sediments, indicating distributed lateral compaction in addition to folding (Moore et al., 2001a; Bangs and Gulick, 2005). The detachment fold extends laterally for at least 75 km with an amplitude that decreases east and west from the Cape Muroto transect, according to seismic surveys and bathymetric maps (Le Pichon et al., 1987; Moore et al., 1990, 2001a; Gulick et al., 2004). The next two landward structures within the wedge are shear fault-bend folds in the hanging walls of thrust ramps, each of which consume about 400 m of shortening and may have begun initially as detachment folds because they show what appear to be truncated detachment folds in the footwall (Suppe et al., 2004; Shaw et al., 2005).

The stratigraphic sequence is well characterized based on cores and logging from Ocean Drilling Project holes ODP-808 and 1174 (Fig. 4) that reached oceanic crust at two sites along our section (Shipboard-Scientific-Party, 2001a,b). The stratigraphy consists of a basal pelagic and hemipelagic sequence of the Shikoku basin that is overlain by distal and proximal trench-fill turbidites (Fig. 5). The lower half of the pelagic–hemipelagic sequence is seismically transparent and overlain by a strong pair of reflectors that lie just below the basal detachment fault, as shown by ODP cores and logs (Figs. 4 and 5). The overlying Shikoku basin hemipelagic sediments show discontinuous seismic reflectors associated with an upward transition into the more proximal trench-fill turbidite sequence with more continuous reflectors (Moore et al., 2001a; Shipboard-Scientific-Party, 2001b).

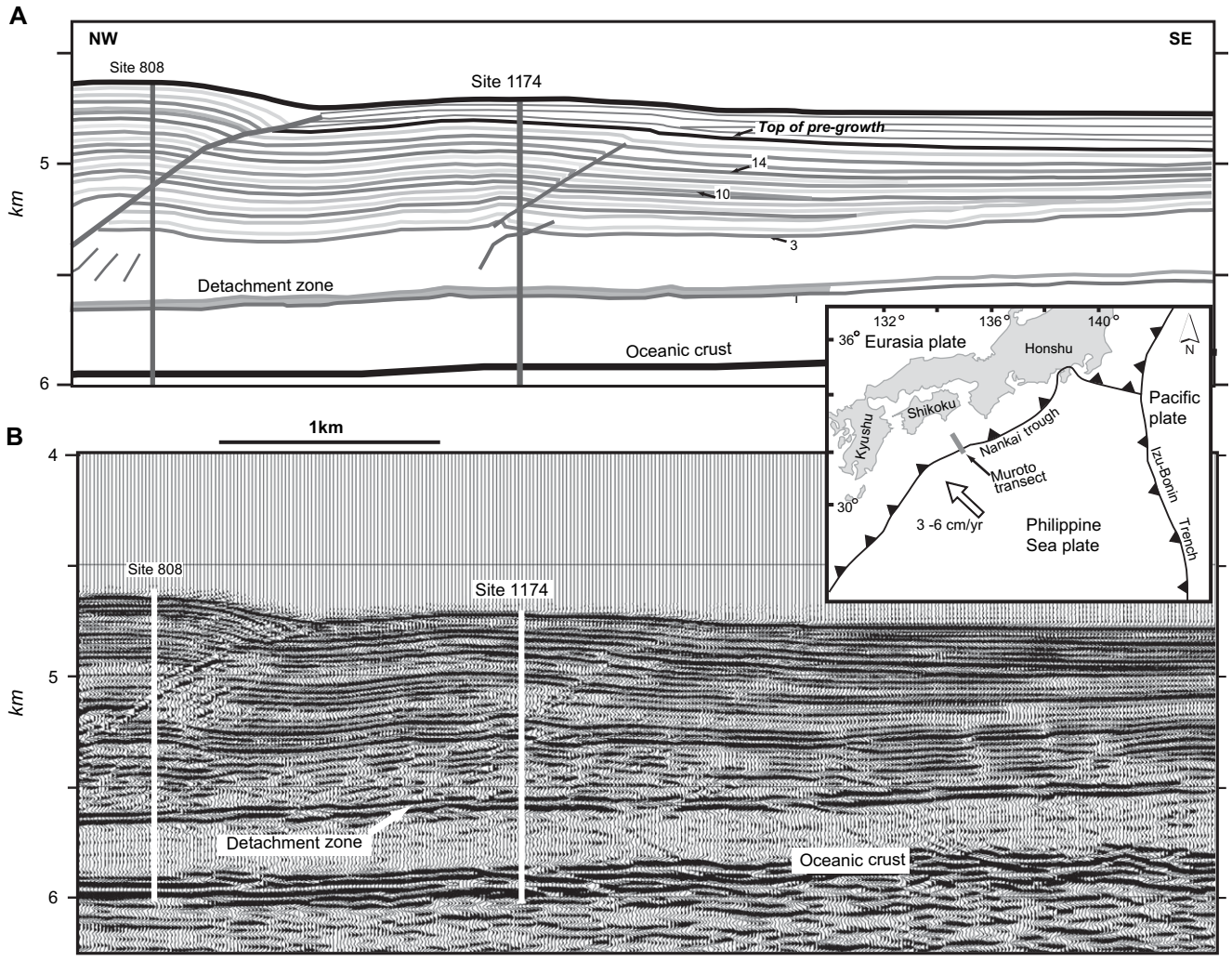

Fig. 4. The frontal detachment fold of the protothrust zone of the Nankai trough, Japan. (A) Interpretation of the seismic profile and locations of ODP boreholes, sites 808 and 1174. Horizon numbers are indicated. (B) Depth-migrated seismic profile (Moore et al., 1991; line 62-8, $h = v$).

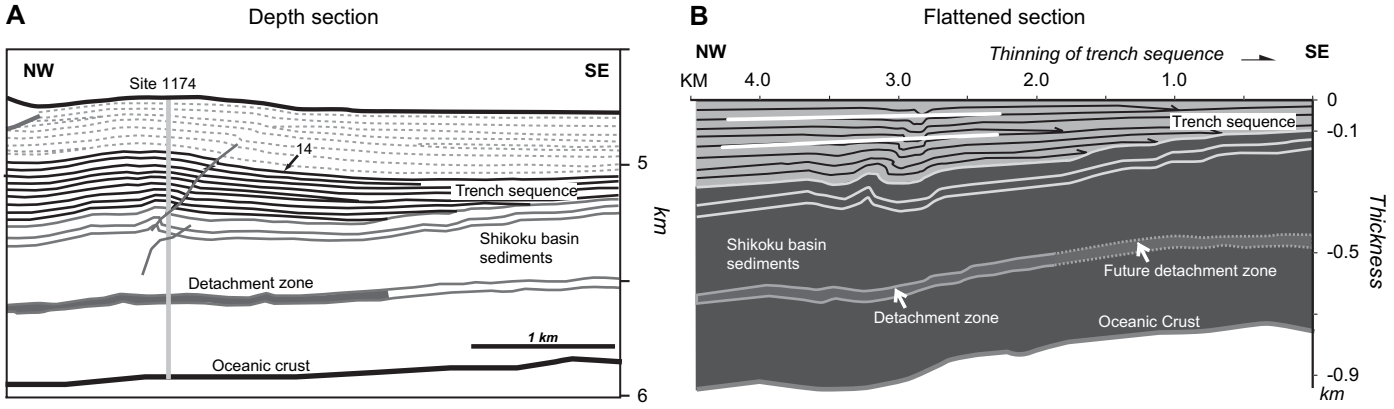

Fig. 5. Cross-section and flattened section of the frontal detachment fold of the Nankai trough, Japan. (A) Depth section showing the main stratigraphic intervals above oceanic crust. (B) The stratigraphic architecture of the basin is more obvious when the section flattened to horizon 14 (Fig. 4), which is near the top of the pregrowth section. The light gray zone is the trench-fill sequence, which thins southward towards the Shikoku basin and shows progradation by onlapping of horizons over part of the Shikoku basin section. The dark gray area is the hemipelagic and pelagic Shikoku basin sequence which contains the detachment zone. White lines show interpreted regional stratigraphic gradients which allow the thickness relief to be measured.

We mapped 26 horizons across the detachment fold using the depth-migrated 2D seismic line NT62-8 (Moore et al., 1990, 1991). The depth of the detachment is well documented from the two ODP holes and has been correlated to the seismic line using synthetic seismograms (Moore et al., 2001a). The maximum limb dips reach about 8° and the landward dip of the detachment horizon is about 1°. In the following section we show in some detail how we transformed these mapped horizons into estimates of shortening $\overline{S}(z)$, $S(z)$ and S_c. Our discussion of the thickness-relief method for this first example is more detailed than for the other three examples, for which we will concentrate largely on the analysis of the results.

4.1.2. Shortening analysis of Nankai detachment fold

The Nankai detachment fold (Fig. 4) is a good example of the need to work in the thickness domain rather than the depth domain. If we attempt to directly interpret the regional stratigraphic gradient for each of the mapped horizons by inspection of the depth section (Figs. 4 and 5a) we see that the choice is rather arbitrary, which makes any direct measurements of area of structural relief in the depth domain intrinsically uncertain. Interpretation of the regional gradient in depth is made more difficult by the regional fanning of dips across the trench and the fact that the back limb of the anticline is elevated relative to the front. Much of this fanning of dip must be stratigraphic, reflecting the filling of the trench and the transition from hemipelagic to trench-fill sedimentation. Therefore we transform the data into the thickness domain by flattening on a through-going horizon high in the pregrowth section, as shown in Fig. 5. In this flattened version of the section we see the main features of the stratigraphic architecture of the trench and are able to easily interpret linear regional gradients, especially in the upper part of the pregrowth sequence. We viewed the structure using a number of flattening horizons before choosing the optimum horizons for the thickness-relief analysis (horizons *OC*, 1, 6, 14, 15, where horizon *OC* is the top of oceanic crust). The thickness-relief data for 18 pregrowth horizons were combined using the methods described in Appendix A to compute the areas of structural relief relative to the detachment horizon as determined by the ODP-1174 borehole (Shipboard-Scientific-Party, 2001b).

The total area of structural relief as a function of height above the detachment is shown in Fig. 6. A linear least-squares fit of the data gives a slope of 77 m, which is the mean shortening $\overline{S}$ for the entire data set. The linear fit passes essentially through the origin in agreement with the location of the basal detachment as determined from drilling and the correlation between the well to the depth seismic line by means of the synthetic seismogram. These results suggest a constant shortening as a function of height above the detachment. This interpretation is supported by the fact that fitting by a second degree polynomial gives a nearly identical maximum shortening of 78 m at the top of the pregrowth section and a bedding-parallel simple-shear angle of less than a degree (Fig. 6b).

Therefore, the data taken as a whole give a nearly constant shortening above the detachment $\overline{S}$ of about 77 m with a small formal error of ±6 m. However, it is still possible that there could be some finer-scale heterogeneity in the shortening as a function of height, $\overline{S}(z)$ or $S(z)$, that does not appear in simple linear or polynomial fitting of the data. The computation of mean shortening $\overline{S}(z)$ for each data point does not reveal any striking heterogeneity nor does the computation of $S(z)$ from the polynomial fit (Fig. 6). Nevertheless the area of relief data in the height range of 400–550 m above the detachment shows less scatter than the rest of the data and may be fit to a substantially lower slope. The possibility that this apparent heterogeneity could represent true structure rather than noise is discussed further below.

We have computed the curvimetric shortening S_c for each horizon using the methods described in Appendix B and find a value of ~2–3 m, which is nearly constant as a function of height and represents only 3% of the shortening $S(z) = \overline{S}(z)$ of about 77 m (Fig. 6b). Therefore only about 3% of the shortening is associated with deflection of the layers from their regional gradient and about 97% of the total shortening is due to layer-parallel shortening with essentially no layer-parallel

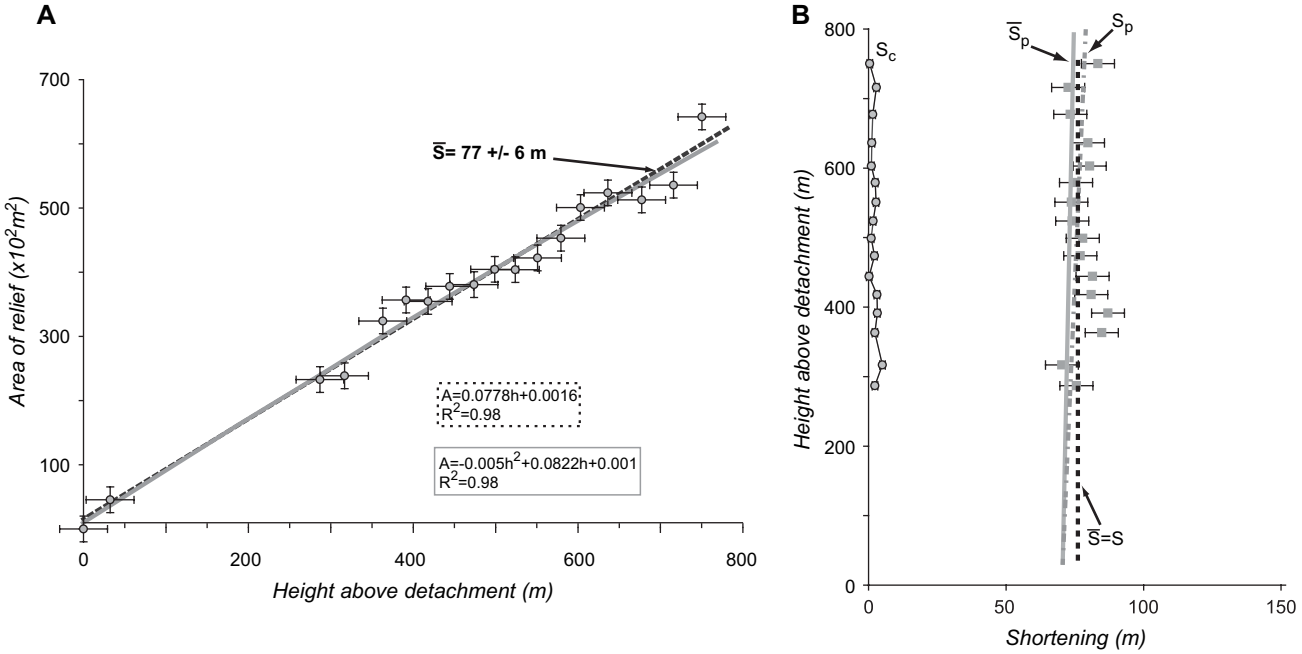

Fig. 6. Area of relief and shortening graphs for the pregrowth section of the Nankai trough detachment fold. (A) Area relief as a function of height above the reference level, which is the detachment level ~ 360 m above the top of oceanic crust. The best-fit linear regression is marked by a dashed line, which gives least-squares shortening for the pregrowth section of $\overline{S} = 77 \pm 6$ m with an R^2 of 0.98. The intercept is essentially at the origin which agrees with the observed detachment level in the ODP borehole. The light gray line is a second-order polynomial fit which gives a maximum shortening at the top of the pregrowth section of 78 ± 6 m and an R^2 of 0.98. (B) Shortening as a function of height. The mean shortening calculated for each data point is $\overline{S} = A_{sr}/H_d$. The vertically homogeneous mean shortening $\overline{S} = S$ from the linear regression in A is shown as a vertical black dashed line. The shortening computed from the second-order polynomial fit S_p is shown as a gray dashed line and the mean shortening $\overline{S}_p$ computed by integration of the polynomial fit is shown as a solid gray line. The general agreement of all these measures of shortening indicates that there is no overall layer-parallel simple shear, as discussed in the text. In contrast the curvimetric shortening S_c is only about 3% of the least-squares shortening.

simple shear. In this respect the Nankai detachment fold closely fits the heterogeneous pure shear detachment fold model proposed by Groshong and Epard (1994).

The above shortening analysis based on conservation of area almost certainly does not capture all the shortening because there are several indications that significant tectonic shortening is consumed in the horizontal component of compaction. First, there are substantial horizontal gradients in seismic velocity that are consistent with increasing compaction into the wedge (Bangs and Gulick, 2005). Secondly, Henry et al. (2003) have estimated a substantial horizontal compaction based on borehole analysis of anisotropic electrical conductivity. Their horizontal stretch of ~0.88, if integrated over the 2–3 km width of the fold suggests ~250–350 m of shortening associated with horizontal compaction, which is large relative to the 77 m constant-volume component of the shortening determined in our analysis (Fig. 7). The total shortening due to horizontal compaction in the protothrust zone should be somewhat larger that this estimate because horizontal compaction appears to begin substantially south of the detachment fold based on estimates of porosity from seismic analysis (Bangs and Gulick, 2005).

Finally, we noted above that the area of relief data in the interval from 400 to 550 m above the detachment may show substantially lower shortening ~47 m than the mean value of 77 m obtained from the least-squares fit of the entire data set (Fig. 6a). This observation seems bizarre from a constant-volume perspective. However, if the horizontal tectonic compaction is large, then it is likely that there will be vertical heterogeneity in the fractions of total tectonic shortening that are consumed by tectonic compaction and constant-volume pure shear. The interval 400–550 m is characterized by mudstones interbedded with substantial sandstones and shows hydrostatic fluid pressures; therefore it may be capable of more tectonic compaction than the underlying overpressured mudstone section and the overlying sandstone-rich section. Therefore, it seems plausible that vertical heterogeneity in the constant-volume component may exist within an environment that is one of large-scale vertically homogeneous total shortening.

4.2. Cascadia detachment fold, offshore Oregon

4.2.1. Geological framework

We analyze the active frontal detachment fold at the toe of the Cascadia accretionary wedge, offshore Oregon (Fig. 8), which is associated with oblique subduction of the Juan de Fuca Plate below the North America plate at a rate of ~4 cm/yr along a zone extending from Vancouver Island to northernmost California (Kulm et al., 1984; MacKay et al., 1992; Westbrook et al., 1994). The stratigraphic section entering the Cascadia deformation front is substantially thicker (3–4 km) than the Nankai example (~1 km) and is composed of turbidites in which a well-defined fold-and-thrust belt has developed with substantial along-strike variation in structural styles with both

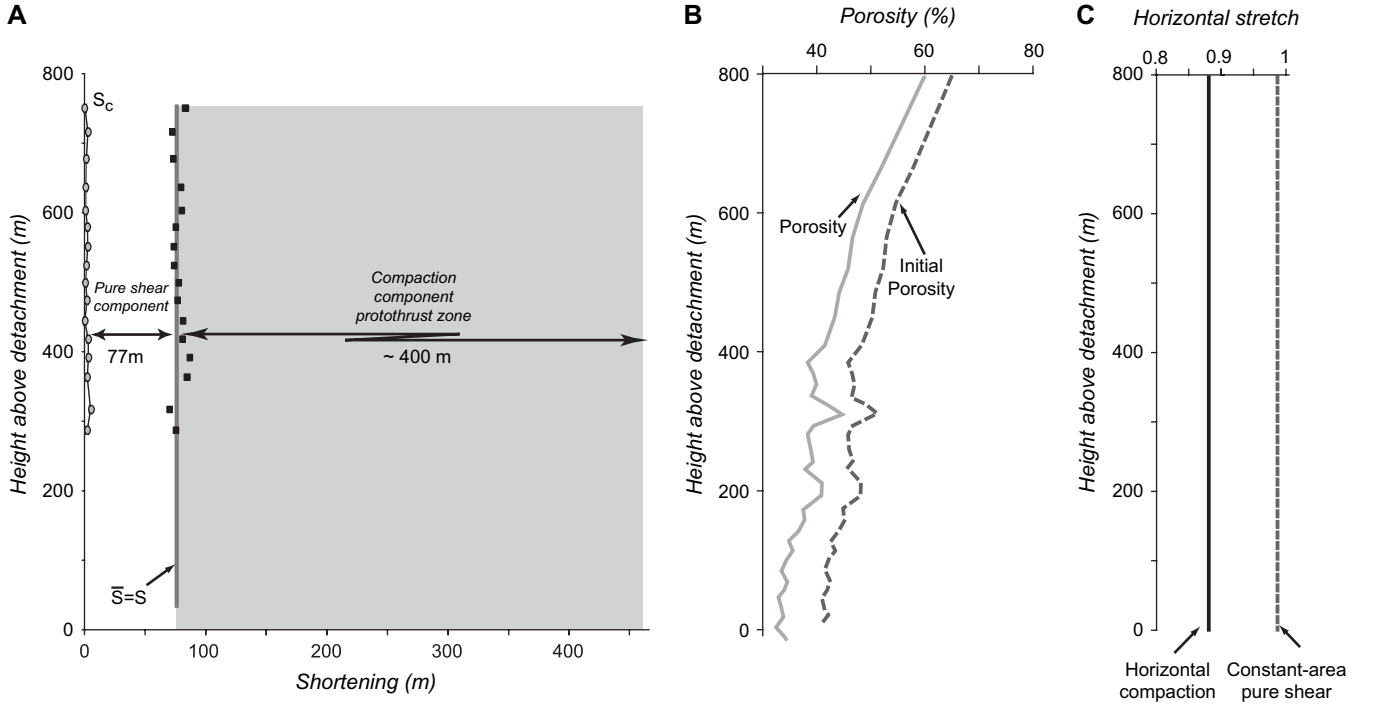

Fig. 7. Components of shortening in the Nankai trough detachment fold. (A) The total shortening is the sum of the constant-volume component of shortening given by the least-squares shortening $\overline{S} = 77$ m and the horizontal compaction component of shortening which is ~400 m for the protothrust zone estimated from horizontal gradients in seismic velocity and porosity (Bangs and Gulick, 2005) and electrical conductivity anisotropy (Henry et al., 2003). The constant-volume component is almost entirely pure shear because the curvimetric shortening S_c is only ~2–3 m (Eq. (7)). (B) Porosity profiles from the ODP-1174 borehole showing the estimated porosity change associated with horizontal compaction (Henry et al., 2003). (C) Stretch profiles for horizontal compaction for the constant area pure shear deformation of the Nankai detachment fold. Stretch for horizontal compaction is calculated by Henry et al. (2003) using electrical conductivity anisotropy.

seaward and landward vergence (Silver, 1972; Kulm et al., 1984; MacKay et al., 1992; MacKay, 1995; Adam et al., 2004).

The site of our study in offshore Oregon is in a region that is similar to Nankai in that it shows a protothrust zone ahead of a seaward-vergent frontal thrust ramp, but the décollement level is not as immediately obvious as in the Japanese case (Fig. 8). The protothrust zone is dominated by a low-amplitude detachment fold just seaward of the frontal thrust ramp, but additional more distributed deformation has been documented as indicated by a landward increase in seismic velocities (Cochrane et al., 1994) and a number of incipient thrust ramps with barely resolvable slip (Fig. 8), studied in detail by Cochrane et al. (1994) and Moore et al. (1995). These incipient thrusts terminate downward at or above the same detachment level as in the main frontal thrust ramp, which Moore et al. (1995) have traced for at least 10 km along strike in other seismic lines. Our analysis of area of structural relief in the detachment fold identifies this same detachment level, which is about 1300 m above the top of oceanic crust, but also shows a deeper detachment level close to the base of the stratigraphic section, as discussed below.

4.2.2. Shortening analysis of Cascadia detachment fold

We analyzed the shortening of the active frontal detachment fold of the protothrust zone based on mapping 35 horizons on depth-seismic line OR-9 of the Ocean Drilling Project (Westbrook et al., 1994; Carson et al., 1995). This line begins on the abyssal plain 10 km seaward from the frontal thrust ramp and displays a landward-thickening 3–4 km thick sequence of Miocene to Pleistocene sediments (MacKay, 1995). Our thickness-relief analysis presented here (Fig. 8) extends downward from the top of pregrowth strata (horizon 23) to the first horizon above the top of oceanic crust (horizon 1). The area relief data as a function of height show a more complex pattern than the Nankai example, with an upward steepening slope indicating that shortening is not constant as a function of height (Fig. 9).

We begin our analysis by noting that there is a rather abrupt overall change in slope of the area–height graph at about 1100 m (~1300 m above top of oceanic crust), which is approximately the horizon of the detachment of the main frontal ramp and the protodetachment of Cochrane et al. (1994). Therefore it is likely that two detachment levels exist (compare Fig. 2). For this reason we analyze the data above and below this level independently, starting with linear regression. Fitting the data below the proposed detachment we obtain a slope corresponding to a mean shortening $\overline{S}_{\text{lower}}$ of 84 m and a zero-area intercept of about 280 m above the top of oceanic crust, which is therefore the level for a lower detachment assuming homogeneous shortening above the detachment. If there were a zone of distributed simple shear in the basal layer (compare Fig. 1) then 280 m would be an upper bound on the base of the deformation and the top of the oceanic crust would presumably be a lower bound. Regression of the upper data set yields a slope corresponding to a mean shortening of the upper block $\overline{S}_{\text{upper}}$ of 256 m. We

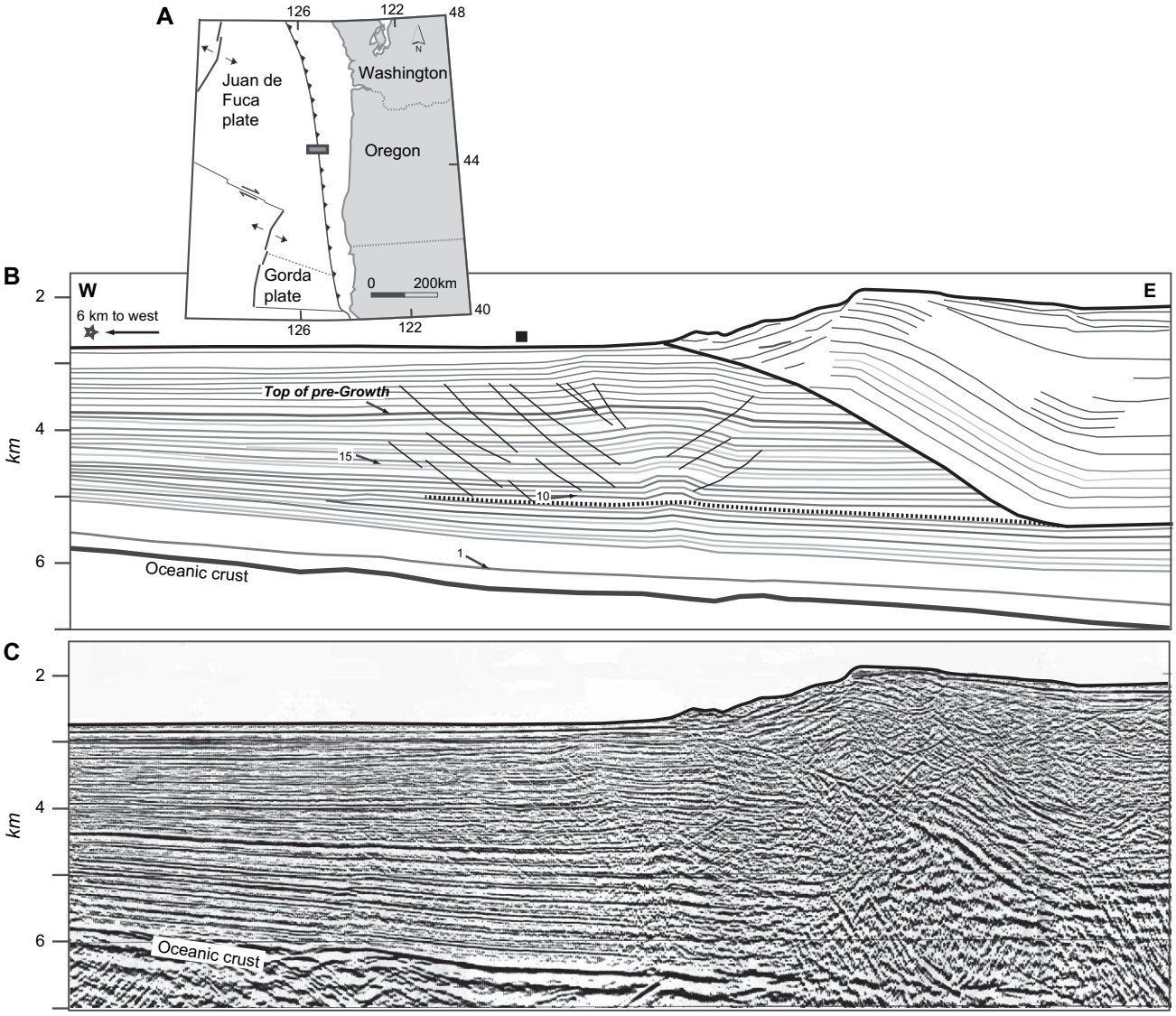

Fig. 8. The frontal detachment fold of the protothrust zone of the Cascadia accretionary complex, offshore Oregon. (A) Regional map showing the location of the seismic profile. (B) Interpretation of seismic profile with horizon numbers shown. The black square and the star are locations of vertical seismic profiles (Cochrane et al., 1994) used to calculate porosity and evaluate horizontal compaction. (C) Depth seismic profile OR-9 (Westbrook et al., 1994; $h = v$).

estimate the location of the upper detachment at about 1284 m above the top of oceanic crust from the intersection of the two linear regressions. This intersection is very close, ~20 m below, to the detachment horizon interpreted independently by Cochrane et al. (1994) for the frontal thrust ramp and protodetachment.

It is important to notice that the 256 m mean shortening $\overline{S}_{\text{upper}}$ obtained by linear regression of the upper strata (Fig. 9) is the sum of the 84 m shortening of the lower strata $\overline{S}_{\text{lower}}$ plus an additional 172 m shortening ΔS that is confined to the upper fault block

$$\overline{S}_{\text{upper}} = \overline{S}_{\text{lower}} + \Delta S$$

This is because the area of relief $A(z)_{\text{upper}}$ at some height H_{upper} above the upper detachment is the sum of the area contributions from the two fault blocks (Fig. 9)

$$A(z)_{\text{upper}} = \overline{S}_{\text{lower}} H_{\text{lower}} + \Delta S H_{\text{upper}}$$

where H_{lower} is the height of the horizon above the lower detachment and ΔS is the slip on the upper detachment that is consumed in constant area folding.

The above analysis involves linear regression and therefore assumes a constant shortening as a function of height within each fault block. We now consider the possibility that there may be some component of homogeneous simple shear within either fault block. Fitting the upper data set with a second-degree polynomial and differentiating yields a maximum *polynomial shortening* $S_{\text{p}}(z)$ at the top of the pregrowth section of 185 m relative to the upper detachment level and a negligible shear profile of 1.8°, suggesting simple shear is not important. Furthermore the mean shortening as a function of height computed from the polynomial $\overline{S}_{\text{p}}(z)$ does not agree well with the observed $\overline{S}(z)$ data, whereas the mean shortening computed

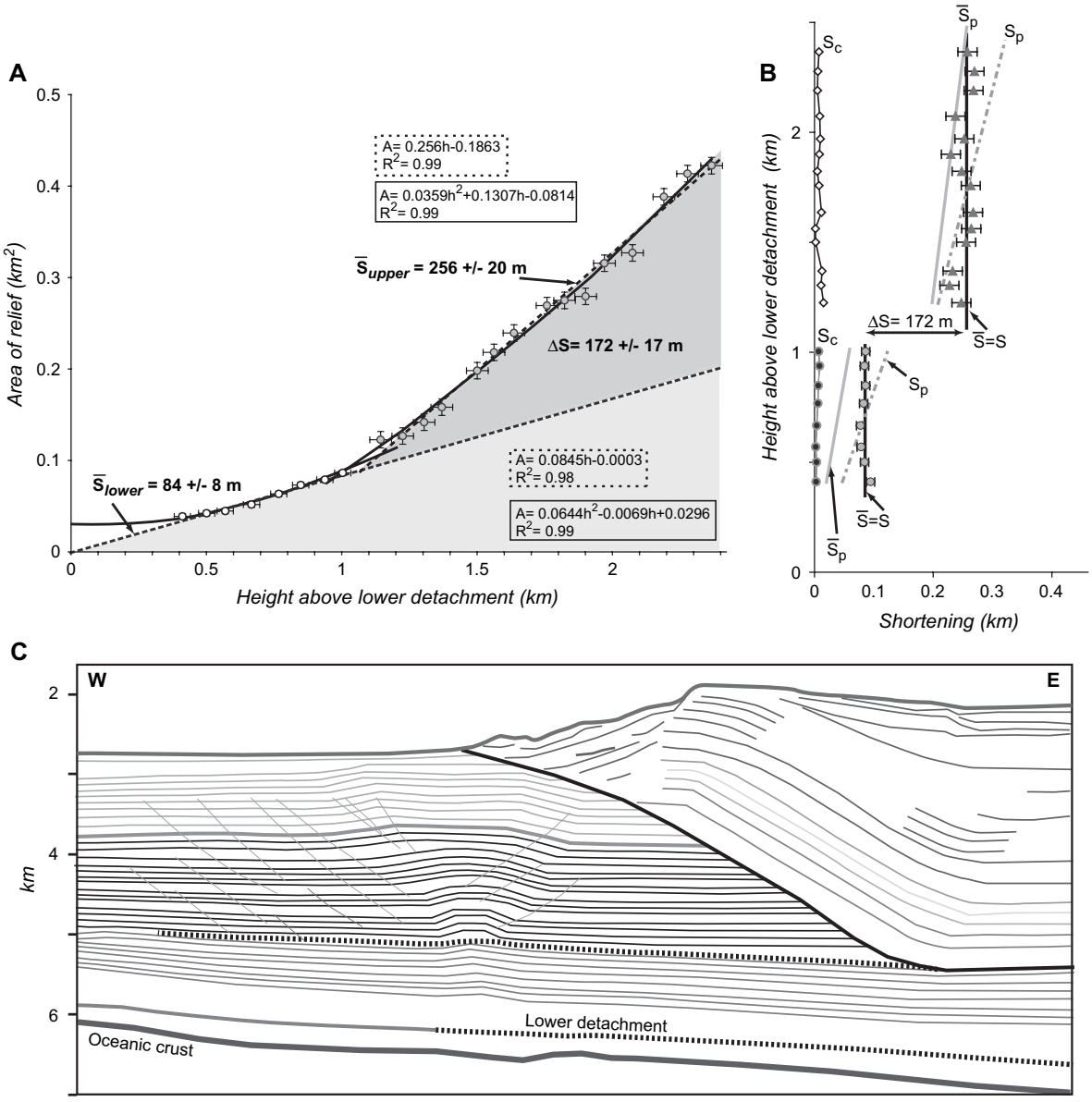

Fig. 9. Area of relief and shortening graphs for the Cascadia detachment fold with revised interpretation of detachments. (A) Area of relief graph. Reference level is ~200 m above the top of oceanic crust, which is the first undeformed horizon. The area of relief data shows two quasilinear trends similar to Fig. 2 suggesting the possibility of two detachments. The data are fit to linear and polynomial trends for each interval, with the black dashed lines indicating linear regression. The lower strata show a linear regression shortening $\overline{S}_{\text{lower}}$ of 84 ± 8 m with a R^2 of 0.98. The upper linear regression has a slope of 256 ± 20 m which represents the total shortening $\overline{S}_{\text{upper}}$ of the upper strata. The difference $\Delta S = 172 \pm 17$ m is the slip on the upper detachment consumed in folding. The intersection of the linear regressions gives an upper detachment level at 1084 m above the reference level. The solid black lines give the second-order polynomial fits, discussed in the text. (B) Shortening graph. The vertically homogeneous mean shortening from both linear regressions $\overline{S} = S$ agrees well with mean shortening computed for the data points; in contrast the mean polynomial shortenings $\overline{S}_{\text{p}}$ disagree. Therefore, we conclude there is no overall layer-parallel simple shear within either the upper or lower strata. The curvimetric shortening S_{c} represents only ~3% the shortening for the upper sequence and 6% of the shortening for the lower sequence, therefore the shortening is dominated by layer-parallel pure shear (Eq. (7)). (C) Reinterpretation of the seismic line using information obtained from the area relief and shortening graphs. The lower detachment is interpreted to be at the reference level (~280 m above the top of oceanic crust) based on the zero intercept of the linear regression.

from the linear regression is in better agreement with the data (Fig. 9). Therefore no overall simple shear exists within the upper fault block.

Fitting the lower data set with a second-degree polynomial and differentiating yields a maximum polynomial shortening $S_{\text{p}}(z)$ at the top of the section of 123 m and a simple shear angle of 7°. However, the predicted mean polynomial shortening as a function of height $\overline{S}_{\text{p}}(z)$ does not agree well with the observed $\overline{S}(z)$ data, whereas the mean shortening computed from the linear regression is in good agreement with the data (Fig. 9). Therefore, there appears to be no overall simple shear within the lower fault block.

The curvimetric shortening was computed from the thickness-relief data using the methods of Appendix B. The lower fault block shows a mean curvimetric shortening of 5 m which is only 6% of the mean shortening $\overline{S}_{\text{lower}}$ of 84 m. The upper fault block shows a total mean curvimetric shortening of 8 m which is only 3% of the linear-regression mean shortening

$\overline{S}_{upper}$ of 256 m. Therefore the Cascadia detachment fold is dominated by pure shear layer-parallel shortening with no simple shear and approximates the Groshong and Epard (1994) pure shear detachment-fold model.

It is also possible that there is a significant component of horizontal compaction in the total tectonic shortening, similar to Nankai, based on the observed horizontal velocity gradients in the protothrust zone (Cochrane et al., 1994). We calculate porosity (Fig. 10b) and associated horizontal stretch (Fig. 10c) from horizontal gradients in velocity using empirical relationships (Hamilton, 1978; Serra, 1984). The computed horizontal stretch due to compaction is ~0.9, which is similar to the constant-volume pure shear stretch. However, the total shortening due to compaction over the entire 6 km width of the protothrust zone is 300–600 m (Fig. 10), which is substantial relative to the 256 m constant-volume pure shear shortening of the detachment fold. Therefore both Nankai and Cascadia show evidence of substantial horizontal compaction.

4.3. Yakeng detachment fold, southern Tianshan China

4.3.1. Geological framework

The active Yakeng anticline (Fig. 11) is located near the town of Kuche at the deformation front of the southern Tianshan fold-and-thrust belt, western China (Hubert-Ferrari et al., 2005). This fold extends for ~100 km along strike and is typically expressed at the surface as a gentle 5–10 km wide and 50–150 m high up warped alluvial surfaces that show abundant evidence of folded pre-existing drainage systems (Hubert-Ferrari et al., 2005, in press). In the few locations of deeper incision, bedding dips in outcrop reach a maximum of about 4–6°. Seismic imaging shows that slip is fed into the Yakeng anticline from Quilitak anticline to the north along a detachment in the Oligocene–Miocene evaporitic Jidikeh Formation (Hubert-Ferrari et al., in press). The depth of the detachment under Yakeng anticline is 5.5–6 km and has been penetrated by several boreholes (Fig. 11). To the south of Yakeng anticline the basement-involved Yanan structure also folds upper Tertiary strata, but shows no surface expression.

4.3.2. Shortening analysis of Yakeng detachment fold

The thickness-relief method was first proposed and applied by Hubert-Ferrari et al. (2005) as part of an analysis of the Yakeng anticline. They determined $\overline{S}(z)$ within both the growth and pregrowth strata and measured the excess area of the fold core A_e associated with flow within the basal evaporitic layer (*cf.* Eq. (5)). Here we use their seismic mapping to extend the analysis of Yakeng by computing additional

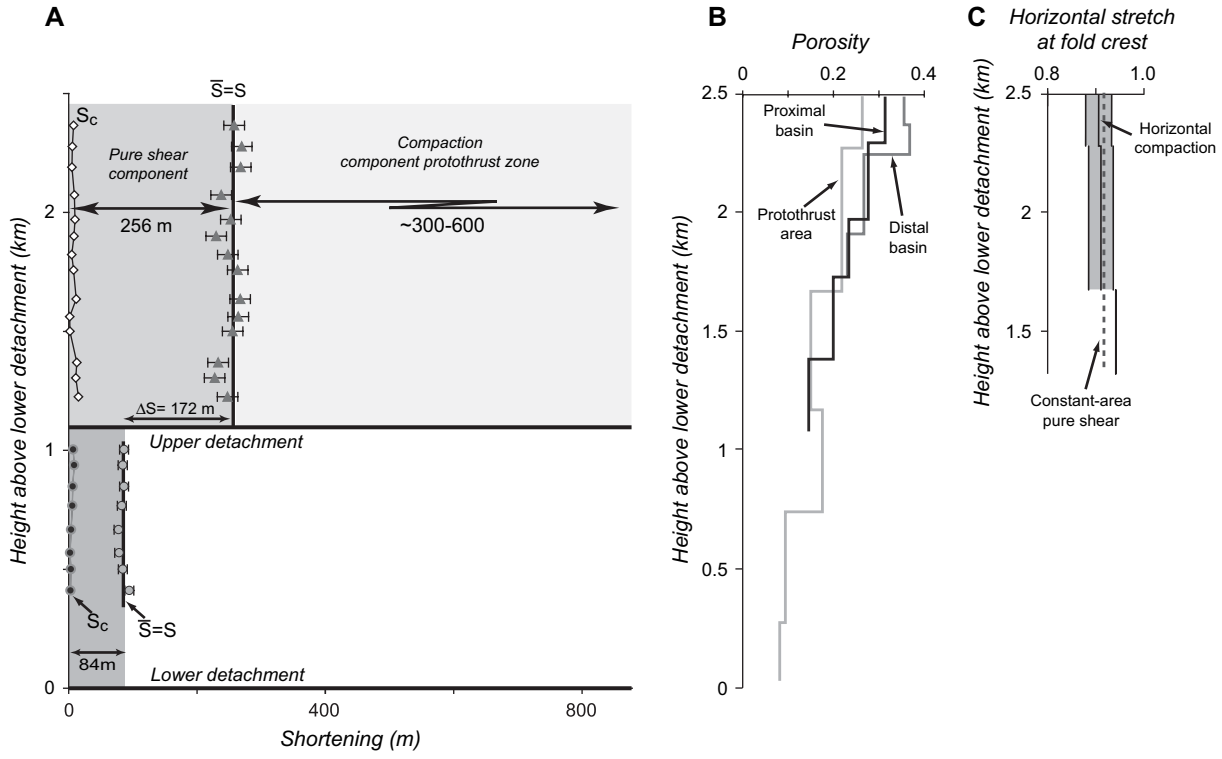

Fig. 10. Components of shortening for the Cascadia detachment fold. (A) The total shortening is the sum of the constant-volume component of shortening given by the least-squares shortening $\overline{S} = 256$ m above the upper detachment and the compaction component of shortening which is ~300–600 m for the protothrust zone estimated from horizontal gradients in seismic velocity (Cochrane et al., 1994). The constant-volume component is almost entirely pure shear because the flexural component given by the curvimetric shortening S_c is only ~8 m above the upper detachment and ~5 m below (see Eq. (7)). (B) Porosity profiles calculated from three velocity profiles from Cochrane et al. (1994) using velocity–density–porosity relationships (see text). Note that porosity decreases toward the deformation front indicating horizontal compaction. (C) Stretch profile for horizontal compaction showing the minimum, mean, and maximum horizontal stretch above the upper detachment. Below 1.7 km the stretch is only calculated from the protothrust and the proximal basin profiles. The dashed line is the stretch value due to pure shear deformation.

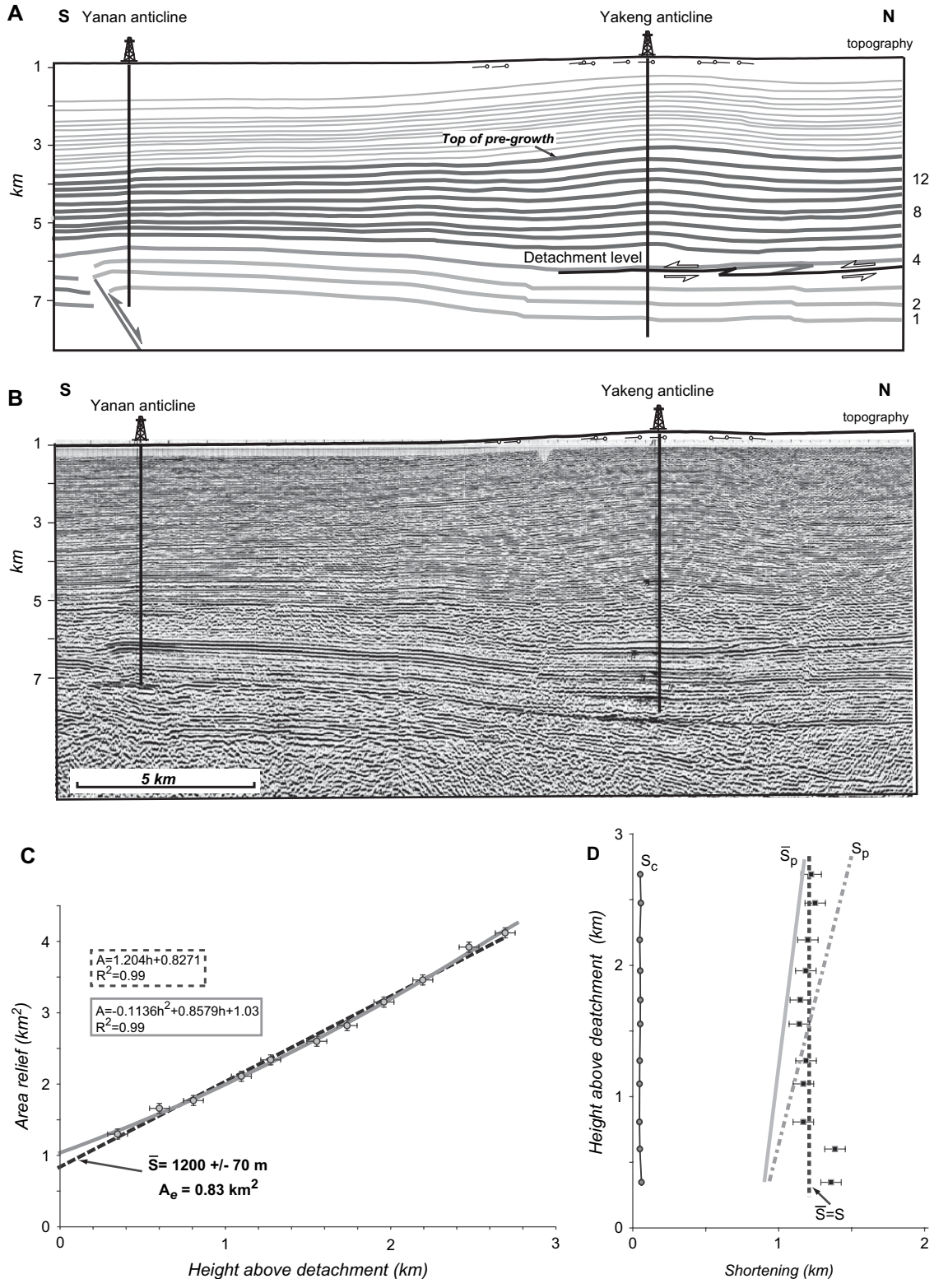

Fig. 11. Yakeng anticline, southern Tianshan, China (after Hubert-Ferrari et al., 2005, AAPG©2005, reprinted by permission of the AAPG whose permission is require for further use). (A) Interpretation of Yakeng detachment fold and Yanan basement inversion structure. Horizon numbers are indicated. (B) Seismic profile. (C) Area of relief graph for Yakeng anticline. The dashed line is the linear regression, which gives a mean shortening $\overline{S}$ of 1200 ± 70 m with an R^2 of 0.99. Note that the zero intercept indicates an excess area of A_e of the fold core of 0.83 ± 0.07 km^2, which is interpreted to be associated with flow of the basal evaporitic interval. The gray line is a second-order polynomial fit, which gives a maximum shortening of 1500 m with an excess area A_e of 1.03 km^2. (D) Shortening graph. The vertically homogeneous shortening $\overline{S} = S$ obtained from the linear regression in C agrees well with mean shortening $\overline{S}$ computed for the data points (Eq. (5)); in contrast the mean polynomial shortening $\overline{S}_p$ disagrees. Therefore we conclude there is no overall layer-parallel simple shear. The curvimetric shortening S_c represents only ~4% the shortening, therefore the shortening is dominated by layer-parallel pure shear (see Eq. (7)).

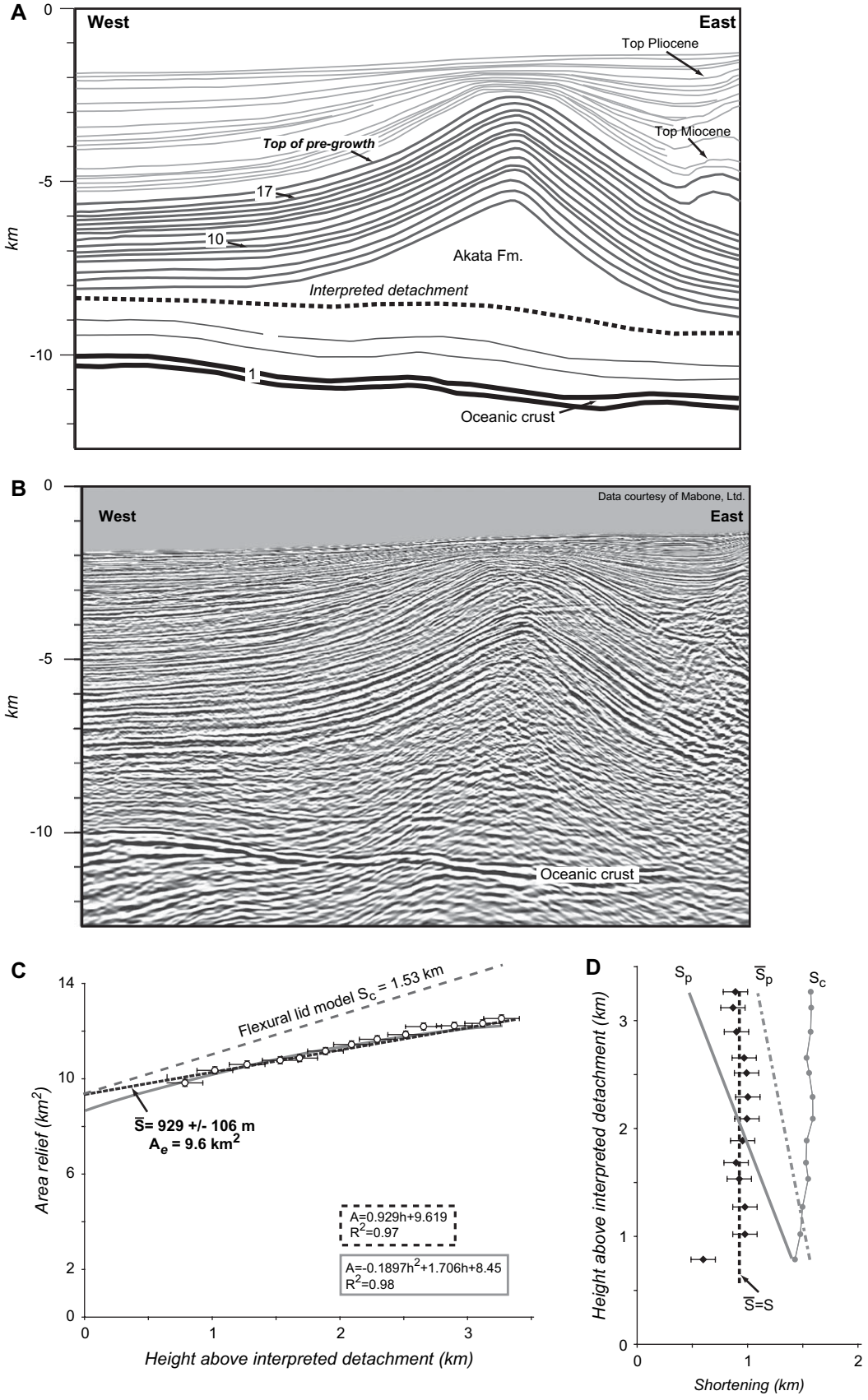

Fig. 12. Agbami anticline offshore Niger delta. (A) Interpretation of the seismic profile. Horizon numbers are indicated. The dashed line represents an assumed detachment level interpreted in the poorly-imaged core of the fold. (B) Seismic profile Agbami anticline (Bilotti et al., 2005, AAPG©2005, reprinted by permission of the AAPG whose permission is require for further use). (C) Area of relief graph. Note that the linear regression gives a very large excess area A_e to the fold core of

components of the shortening as a function of height within the pregrowth strata.

Twenty-seven horizons were mapped by Hubert-Ferrari et al. (2005) for their thickness-relief analysis, which involved several flattening horizons. Here we analyze the interval from the detachment horizon 4 to the uppermost pregrowth horizon 15. The area of relief as a function of height above the detachment is shown in Fig. 11. Fitting this linear array of data to a regression we obtain a mean shortening $\overline{S}$ of 1200 m. Note, however that the regression line does not intersect close to the origin of the graph and shows an excess area of the fold core at the detachment level of 0.8 km^2. Hubert-Ferrari et al. (2005) showed that there was substantial thickness variation within the interval between horizons 4 and 5 and therefore interpreted this excess area A_e to be the result of net flow of the basal evaporitic Jidikeh Formation into the core of the fold. This excess area represents a constant area that is added to all overlying pregrowth horizons as described by Eq. (5), which is used to compute the shortening $\overline{S}(z)$. If we compare the mean shortening from the linear regression with the mean shortening computed for each data point (Fig. 11) we see that they are in good agreement, except that horizons 5 and 6 show ~100 m more computed shortening, which may indicated that excess area A_e in the fold core extends up as high as horizon 6.

We explore the possibility of a layer-parallel simple-shear component by fitting the data to a second degree polynomial, obtaining a shortening $S_p(z)$ that reaches 1.5 km at the top of the pregrowth sequence (horizon 15), a simple-shear angle of 13°, an excess area A_e at the fold core of 1.03 km^2 (Fig. 11). However, the predicted mean shortening $\overline{S}_p(z)$ computed from the polynomial does not agree with the mean shortening $\overline{S}(z)$ computed for each data point, whereas the linear regression agrees well (Fig. 11). Therefore, we conclude that there is no overall simple shear within the pregrowth strata.

We computed the curvimetric shortening $S_c(z)$ for each horizon using the methods described in Appendix B and find a mean value of ~50 m, which is nearly constant as a function of height and represents only about 4% of the total least-squares shortening $\overline{S}$ of about 1200 m (Fig. 11). Therefore the Yakeng detachment fold is dominated by layer-parallel shortening (heterogeneous pure-shear), similar to the pure shear model of Groshong and Epard (1994), with a constant addition to the fold amplitude associated with a net flow of the basal evaporitic Jidikeh Formation into the fold core.

4.4. Agbami detachment fold, Niger delta

4.4.1. Geologic framework

The Agbami detachment fold (Fig. 12) lies at 1500 m water depth within the passive-margin fold-and-thrust belt of the Niger delta, offshore Nigeria, and contains one of the largest petroleum discoveries of the last decade (Grimes et al., 2004). The stratigraphic thickness reaches 9–10 km, composed of an upper well-imaged Miocene to Recent turbiditic section (0–17 Ma) overlying a 2–3 km thick seismically poorly-imaged basal section dominated by pro-delta shales of the Akata Formation (Bilotti et al., 2005). The Akata Formation is thought to be highly overpressured and forms the main detachment of the Niger delta, dominating its mechanics (Bilotti and Shaw, 2005; Corredor et al., 2005a). In some structures the Akata Formation has been interpreted as highly mobile or diapiric (Cohen and McClay, 1996; Hooper et al., 2002).

The Agbami detachment fold is ~10 km wide with substantially higher amplitude and limb dips than our previous examples (Fig. 12). A strong ~4–5° landward-dipping reflector at 10–11 km depth is determined to be the top of oceanic basement as shown by magnetic depth-to-basement calculations (Bilotti et al., 2005; Corredor et al., 2005b). The landward regional dip causes the west limb of this otherwise symmetric anticline to have lower dip (~25°) compared with the east limb (~35°). The back limb of the anticline is deformed by a poorly-imaged fault-related fold and restricts the continuity of the east flank. The shallow reflectors within the growth strata show substantial limb rotation, combined with limb widening (Bilotti et al., 2005).

The exact nature and level of the detachment are not clearly seen because of problems of multiples in the seismic imaging (Grimes et al., 2004), nevertheless faint reflectors are apparently visible as much as 2 km shallower than the top of oceanic crust and subparallel to it, suggesting a detachment at that level (Fig. 12). Our interpreted detachment is ~1 km shallower than that interpreted by Bilotti et al. (2005), but other structurally interesting interpretations are also possible, as discussed below. In any case the strata above the top of the Akata Formation display a well-defined flexural lid, whereas the core of the fold in the Akata Formation shows a very substantial excess area regardless of the interpreted detachment level. Our thickness-relief analysis will allow us to quantify this behavior.

4.4.2. Shortening analysis of Agbami detachment fold

Thirty-five reflectors were mapped between the top of oceanic crust and the sea bottom (Fig. 12). The top of the pregrowth sequence is at reflector 19 based on an upward decrease in structural relief, however, we exclude horizons 18 and 19 from our analysis of pregrowth strata because they are involved in secondary folding on the east flank of the structure. Four different flattening levels were used to obtain the thickness-relief data. We have combined these data

~9.6 km^2, whereas the shortening of the overlying lid is only 929 ± 106 m. The dashed line of higher slope shows the predicted gradient in the area of relief in the case of a flexural deformation of the lid sequence above the fold core ($S = S_c$), which disagrees with the data, indicating that the deformation of the lid sequence is not dominated by flexure. The polynomial regression is shown as a gray line. (D) Shortening graph. The vertically-homogeneous shortening $\overline{S} = S$ from the linear regression in C agrees well with mean shortening $\overline{S}$ computed for the data points; in contrast the mean polynomial shortening $\overline{S}_p$ disagrees. Therefore, we conclude there is no overall layer-parallel simple shear within the lid sequence. The observation that the curvimetric shortening S_c exceeds the shortening $\overline{S} = S$ of the lid sequence by ~160% indicates that there is substantial layer-parallel stretching of the lid sequence induced by the excess area of the fold core, as discussed in the text.

using the method of Appendix A to present the data as areas of structural relief relative to our interpreted detachment level. Similar to our other examples, the Agbami data display a broadly linear trend that can be fit with either a linear regression or a second-degree polynomial. The slope of the data is so low that the excess area of the fold core at the detachment level is relatively insensitive to the choice of the detachment level or the functional fit to the data (Fig. 12). The excess area of the fold core A_e is $\sim$9–10 km^2.

Linear regression of the relief data yields a mean shortening $\overline{S}$ of the competent lid of 929 m. The intercept yields an excess area A_e of the fold core of 9.6 km^2 for our choice of detachment (Fig. 12) and 8.7 km^2 for the $\sim$1 km deeper detachment interpreted by Bilotti et al. (2005). We can compute the mean shortening $\overline{S}(z)$ for each data point using Eq. (5)

$$\overline{S}(z) = (A_{sr} - A_e)/H_d$$

which attempts to remove the effect of excess area A_e from the estimate of mean shortening for each data point. The computed $\overline{S}(z)$ for the individual data points agree closely with the mean shortening $\overline{S}$ from the linear regression, indicating that the shortening within the flexural lid is nearly constant as a function of stratigraphic level, with essentially no overall simple shear (Fig. 12). Only for the lowest data point does $\overline{S}(z)$ deviate substantially from the mean shortening $\overline{S}$.

We further test this conclusion of no simple shear by performing a second-degree polynomial fit to the area of relief data (Fig. 12), which we differentiate to obtain the polynomial shortening $S_p(z)$ as a function of height. The result is a negative shear of 13° and a shortening $S_p(z)$ that decreases from 1190 m at the base of the lid to 589 m at horizon 17. The mean shortening $\overline{S}_p(z)$ computed from the polynomial fit agrees poorly with the mean shortening for the data points (Fig. 12), confirming our conclusion from the linear regression of constant shortening as a function of height with no simple shear.

We computed the curvimetric shortening $S_c(z)$ for each horizon using the methods described in Appendix B and find a mean value of $\sim$1.53 km with a slight upward increase in the 1 km section above the top of the Akata Formation (Fig. 12). This value is substantially greater than the shortening $S \approx \overline{S}$ of 0.93 km measured from the relief data, but is approximately that predicted for deflection above the observed excess area, therefore $S_c(z)$ is dominated by deflection above the fold core. The total layer-parallel shortening consumed within the flexural lid is related to the curvimetric shortening S_c by Eq. (7)

$$S = S_c + S_\varepsilon = S_c + (S_{\varepsilon_{lid}} + S_{\varepsilon_A})$$

where the net change in bed length S_ε is the sum of any pure shear shortening of the lid $S_{\varepsilon_{lid}}$ plus the stretching of the lid above the excess area S_{ε_A}. Note that because of the substantial limb dip in Agbami the layer-parallel shortening of the lid $S_{\varepsilon_{lid}}$ may be different from the *horizontal* shortening measured from the area of relief $S \approx \overline{S}$. We consider two cases: [1] If the horizontal shortening is early before the excess area develops then the two are equal, $S \approx S_{\varepsilon_{lid}} = 0.93$ km, $S_{\varepsilon_A} = -1.53$ km and $S_\varepsilon = -0.6$ km. [2] If the horizontal shortening is late, after the excess area develops, then the layer-parallel shortening $S_{\varepsilon_{lid}}$ associated with a final dip of 35° is $S_{\varepsilon_{lid}} \approx 0.5$ km, $S_{\varepsilon_A} = -1.1$ km, and $S_\varepsilon = -0.6$ km. Thus the net change in bed length is $S_\varepsilon = -0.6$ km for these two cases, where the negative sign indicates an increase in bed length (shortening is positive). Therefore, the layer-parallel stretching of the lid dominates over any pure shear shortening because $|S_{\varepsilon_A}| > S_{\varepsilon_{lid}}$.

In contrast, we can rule out the possibility of a true flexural lid with conservation of bed length for Agbami, which would predict a 65% larger vertical gradient in area of relief (Fig. 12c). The deformation of the lid sequence of Agbami is therefore different from existing flexural detachment fold models that conserve bed length (Mitra and Namson, 1989; Dahlstrom, 1990; Homza and Wallace, 1995; Poblet and McClay, 1996; Suppe, submitted for publication) because the deflection of the Agbami lid is dominated by layer-parallel stretching over the excess area of the fold core. We conclude that the area of structural relief of the Agbami anticline is dominated by deflection over a fold core with 9–10 km^2 excess area A_e and an associated net stretching S_ε of 0.6 km ($\sim$6–8%); an additional 1–2 km^2 upward-increasing area of relief is associated with $\sim$0.93 km of shortening in the lid and no simple shear.

The origin of the excess area A_e within the Akata Formation is a major problem. The 9–10 km^2 excess area in the basal layer, which appears to be 1–2.5 km thick, requires the equivalent of 4–10 km of shortening to produce the observed excess area of structural relief, in contrast with the $\sim$0.93 km shortening in the overlying strata. This is similar to the classic problem of detachment folding in a mechanical stratigraphy composed of a flexural lid overlying a weak basal layer (Wiltschko and Chapple, 1977; Homza and Wallace, 1995; Suppe, submitted for publication). The classic solution to this problem has been flow of the weak basal layer, such as salt, into the core of the anticline from the adjacent synclines as shown in Fig. 13a (Wiltschko and Chapple, 1977; Homza and Wallace, 1995). This solution of local constant-volume redistribution of the basal layer is not satisfactory for Agbami because the well-imaged syncline west of Agbami does not show the $\sim$1 km average drawdown over a 5 km wide region that would be required. Indeed, no drawdown is seen at all in the thickness relief of either the basal layer or the growth strata.

The Agbami anticline therefore requires another solution to the problem of excess area. The only remaining solutions are those that are open-system solutions involving material entering or exiting the confines of the local structure within the 2D cross-section (Suppe, submitted for publication). There are several possibilities that are most likely in the present context, none of which are easily tested with the present seismic data (Fig. 13):

[1] Far-field injection of mobile Akata shale from the interior of the Niger delta may supply the 9–10 km^2 excess area

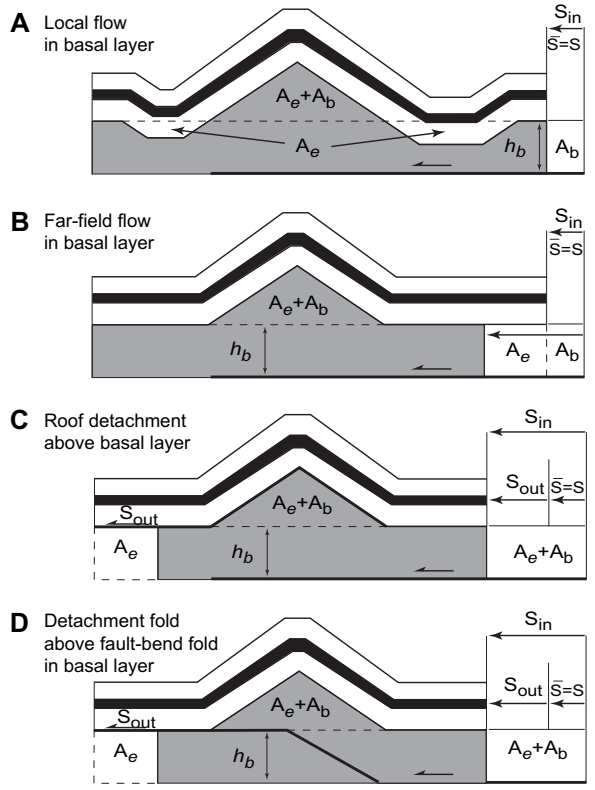

Fig. 13. Open and closed system detachment fold models with excess area A_e in the fold core. (A) Closed system detachment fold with local flow of the basal layer involving deflection of horizons both above and below the regional stratigraphic level. The excess area is equal to the area of subsidence of the synclines. (B) Open system with a far field injection of the basal layer into the core without subsidence of the syncline. (C) Open system with a roof detachment that represents a discontinuity in shortening. The excess area is equal to the difference in area of shortening above and below the roof detachment. (D) Open system with roof detachment similar to (C) but with deformation of the basal layer accomplished by a somewhat flattened fault-bend folding.

(Fig. 13b). In support of this concept are other structures in the Niger delta that have been interpreted as shale diapirs (Hooper et al., 2002). Such far-field flow of shale, while often contemplated by analogy with the flow of salt, is unfortunately not yet a well-tested hypothesis in the literature. There appears to be no specific observable properties of the seismic image that allow us to test this hypothesis in the case of Agbami, however, the observed stretching of the lid sequence is compatible with this idea.

[2] Alternatively the Agbami anticline may involve two detachments, a floor detachment within or at the base of the Akata Formation and a roof detachment near the top of the Akata Formation (Fig. 13c). A variety of solutions of this type allow different shortening above and below the roof detachment, with the difference in shortening taken out of the system on the roof detachment (Suppe, submitted for publication). These solutions are kinematically similar to duplexes. Seismic images of nearby structures show a horizon just below the top of the Akata Formation to be the most important detachment regionally (Corredor et al., 2005a,b). The amount of shortening that must exit the system on the roof detachment depends on the thickness of the basal layer. The minimum thickness is ~1 km using the interpreted detachment of Fig. 12 and ~2 km for the detachment interpreted by Bilotti et al. (2005). The maximum possible thickness is ~2.5 km, which is the height of the Akata Formation above the oceanic crust. A lower detachment close to the top of oceanic crust is most likely because it is observed to be important regionally within the more interior parts of the thrust belt (Corredor et al., 2005a). Therefore, the amount of shortening of the basal layer of 1–2.5 km thickness required to produce the 10 km^2 area of structural relief at the top of the Akata Formation is 4–10 km. Therefore 3–9 km of slip would have to exit the system along the roof detachment at the top of the Akata Formation, since ~0.9 km of shortening is observed above the Akata Formation. Shortening of this magnitude above a detachment near the top of the Akata Formation is observed ~10 km to the west (Shaw et al., 2005) in agreement with this open system solution. This mechanism is apparently compatible with the observed stretching of the lid sequence.

The deformation in the core of the Agbami detachment fold could take a variety of forms, including those that are not normally considered detachment folding, as emphasized by Groshong and Epard (1994). For example the area of relief at the Akata level could be produced as a complex duplex structure between the two detachments or even as a single, somewhat mobile, fault-bend fold stepping up from near the base of the section (Fig. 13d), as long as the lid sequence deforms in a manner consistent with the observed stretching. In all these cases the amount of slip exiting the system on the upper detachment should be approximately the width of the limb of the anticline at the Akata level, which is ~5 km, which is consistent with a lower detachment ~2.5 km below the top of the Akata Formation, near the top of oceanic crust. All of these possible solutions for the origin of Agbami anticline must wait for better seismic imaging. However, the observation of the two required detachments regionally and the upper detachment just to the west confirms the general viability of the open-system solutions (Fig. 13c, d). The thickness-relief results have placed significant quantitative constraints on these considerations.

5. Discussion of methodology

The study of our four examples gives us some initial experience with the application of thickness-relief methods to the analysis of shortening in detachment folds. Here we comment briefly on some methodological concerns over the more general applicability of these methods to well-imaged structures.

The low scatter of the primary measurements of area of relief as a function of height in our examples suggests that the thickness-relief method is capable of giving quite consistent results. The least-squares fitting of the data gives mean shortenings $\overline{S}$ with fitting errors on the order of 10% for shortening

between 77 and 1200 m. Nevertheless we do not have a strong constraint on the resolution of the method in specific cases. In particular we do not know to what extent the existing scatter is measurement error as opposed to true stratigraphic heterogeneity in the area of structural relief. Modest stratigraphic heterogeneity in the area of relief is expected if [1] horizontal tectonic compaction is significant, [2] some layers are capable of layer-parallel flow, or [3] unrecognized detachment horizons or zones of heterogeneous layer-parallel simple shear of modest displacement exist within the structure. Least-squares or polynomial fitting of the data will formally consider such heterogeneous deformation as error.

The simple flattening technique that we used in our application of the thickness-relief concept was relatively easy to apply for our isolated low-amplitude examples. This approach is almost certainly not universally applicable without modification, especially in more complex high-amplitude or recumbent structures. Some structures containing significant faults may require some substantial adjustment in techniques for flattening and for thickness and bed-length measurements. In structures that are not isolated it may be more challenging to determine the regional gradients. Other measures of thickness may be appropriate in these structures, for example bed-normal thickness measurements. Nevertheless, we feel the thickness-relief concept is broadly applicable and its limits have yet to be fully probed.

6. Conclusions about detachment folding

Our analysis of four relatively well-imaged examples using thickness-relief methods provides significant new insight into the nature of shortening as a function of height in detachment folds, which we summarize here. Nevertheless our range of examples does not begin to sample the full rich variety of structural phenomena known to exist in detachment folds (Suppe, submitted for publication). In particular, none of our examples, with the possible exception of Agbami, shows strongly competent mechanical stratigraphy of the sort that that is typical of many classic detachment folds, for example the box folds of the Jura and Pyrenees which are composed of competent Jurassic carbonates overlying Triassic evaporates (Laubscher, 1961, 1965, 1966; Mugnier and Vialon, 1986; Poblet and Hardy, 1995). Our results are for low-amplitude detachment folds in relatively homogeneous clastic-dominated mechanical stratigraphy.

All four examples show relatively modest least-squares shortening $\overline{S}$ ranging from 77 to 1200 m in structures that are 5–10 km wide. This shortening is essentially constant as a function of height with no overall simple shear. The measured shortening $\overline{S}$ or $S(z)$ is almost entirely a result of heterogeneous pure shear in the Nankai, Cascadia and Yakeng examples, as shown by the fact that the curvimetric or bed-length shortening S_c is one or two orders of magnitude smaller than the shortening. Therefore these folds may be approximated by the Groshong and Epard (1994) pure shear model of detachment folding.

The Agbami anticline and, to a lesser degree, the Yakeng anticline are more complex in that they show substantial excess area A_e within the basal layer (1–9 km^2), which causes deflection of the overlying strata. In Agbami this deflection is associated with a net increase in bed length ($S_\varepsilon = -0.6$ km) as shown by the fact that the shortening ($S = \overline{S} = 0.93$ km) is less than the curvimetric shortening ($S_c = 1.53$ km). This shows that the deflection of the overlying strata was dominated by layer-parallel stretching of the layers.

Finally, there is significant evidence that our measured shortening $\overline{S}$ or $S(z)$, based on conservation of area, is less than half of the total tectonic shortening for the frontal detachment folds of the Nankai and Cascadia accretionary wedges. The additional shortening, not seen in the area of relief measurements, is associated with horizontal tectonic compaction and volume loss. The evidence for horizontal compaction comes from horizontal increases in seismic velocity (Cochrane et al., 1994; Bangs and Gulick, 2005) and anisotropy in electrical conductivity (Henry et al., 2003) as one enters the deformation front. Given the relative importance of horizontal compaction at early stages in deformation it is possible that some of the finer-scale heterogeneity in the area of relief measurements could represent stratigraphic variations in the proportion of the shortening that is taken up by horizontal compaction. However, at present, horizontal compaction is a relatively unstudied process.

Acknowledgements

We are grateful to Richard Groshong and Eric Erslev for their thoughtful and encouraging reviews that have helped us improve the manuscript. We thank Aurélia Hubert-Ferrari, Wang Xin, Frank Bilotti, Mathieu Daëron and a number of participants at the International Conference on Fault-Related Folding in Beijing (2005) for stimulating advice and encouragement on this research. We thank Greg F. Moore of the University of Hawaii for providing the seismic image of the Nankai trough. Suppe is grateful to the Tectonic Observatory at Caltech, the Geophysics Section Ludwig Maximilians University Munich and the Alexander von Humboldt Foundation for support during the writing of this paper.

Appendix A. Computation of structural relief from thickness-relief measurements

Our data $\langle x_i, z_{n,x_i} \rangle$ consist of sets of horizon elevations $\langle z_{n,x_i} \rangle$ measured at regularly-spaced horizontal positions $\langle x_i \rangle$ for each of the n mapped horizons. Such data can be obtained easily by mapping stratigraphic horizons on depth-converted seismic profiles using suitable software. We did not use special-purpose seismic-mapping software, but simply used Adobe Illustrator™, extracting the digitized horizons from the ASCII Illustrator™ file, which was then imported as a matrix into spreadsheet software (Excel™). All flattening, determinations of best-fitting regionals, calculations of area of relief, heights and curvimetric shortening, and statistical analysis were done in the spreadsheet software.

The thickness-relief method permits significant flexibility in measuring areas of relief in complex stratigraphic and structural situations because measurements can be made independently for several different stratigraphic intervals within a structure, then later combined if there are layers in common between the data sets. For the sake of clarity, two kinds of reference frames or levels are distinguished, relative to which areas of relief and heights can be measured or computed: [1] The *flattening level* is a stratigraphic horizon that is selected as appropriate for flattening for the purpose of identifying the regional stratigraphic gradients and for making the primary measurements of thickness relief and height (Figs. 3 and 14). [2] In contrast, the *reference level* is a horizon relative to which we would like to view the data. The most useful reference level is the detachment horizon or some well-imaged horizon below the detachment horizon. These reference horizons may or may not be undeformed.

In this Appendix we show how to combine data from different flattening levels to recast the data relative to an appropriate reference level, making use of a convenient system of notation. Our notation indicates a measured area of thickness relief of a horizon n relative to a *flattening level* f as a difference in relief $\Delta A_{f,n}$ with an associated difference in height $\Delta H_{f,n}$ (e.g. $\Delta A_{3,5}\Delta H_{3,5}$ Fig. 14c). In contrast the area of relief and height of a horizon n relative to a *reference level* r is indicated without the Δ as $A_{r,n}$ and $H_{r,n}$ simply because in many cases these will be the total area of structural relief and height relative to the detachment or a horizon below the structure of interest. Thus $A_{r,n}$ is in many cases a classic total area of structural relief whereas the thickness relief $\Delta A_{f,n}$ is typically a difference in relief between easily mapped nearby horizons. In either case the total area of relief $A_{r,n}$ or $\Delta A_{f,n}$ between two horizons r or f and n is simply the sum of the differences in relief $\Delta A_{k,k+1}$ between all the intervening adjacent horizons k and $k+1$

$$A_{r,n} = \Delta A_{r,r+1} + \Delta A_{r+1,r+2} + \cdots + \Delta A_{n-1,n} = \sum_{k=r}^{n-1} \Delta A_{k,k+1} \quad (9a)$$

or

$$\Delta A_{f,n} = \Delta A_{f,f+1} + \Delta A_{f+1,f+2} + \cdots + \Delta A_{n-1,n} = \sum_{k=f}^{n-1} \Delta A_{k,k+1} \quad (9b)$$

Similarly for height

$$H_{r,n} = \Delta H_{r,r+1} + \Delta H_{r+1,r+2} + \cdots + \Delta H_{n-1,n} = \sum_{k=r}^{n-1} \Delta H_{k,k+1} \quad (10a)$$

or

$$\Delta H_{f,n} = \Delta H_{f,f+1} + \Delta H_{f+1,f+2} + \cdots + \Delta H_{n-1,n} = \sum_{k=f}^{n-1} \Delta H_{k,k+1} \quad (10b)$$

where $\Delta H_{k,k+1}$ is the difference in height between adjacent horizons k and $k+1$. Thus we can add two measurements if they have a horizon in common, as shown by the subscripts

$$\Delta A_{m,s} = \Delta A_{m,p} + \Delta A_{p,s} \quad (11)$$

which is the basis for combining measurements from different flattening levels, in this case m and p.

Thickness relief ΔA and height ΔH are positive for horizons above the flattening level and negative for horizons below (Figs. 3 and 14). Also the sign of ΔA reverses for extensional structures because extension creates negative rather than positive structural relief (Groshong, 1994, 1996). If we employ multiple flattening and reference levels it is helpful to be more explicit about sign conventions and the horizon indices. We number the sequence of horizons increasing stratigraphically upward (Fig. 14). Therefore $\Delta A_{f,n}$ is positive in compression if $f < n$ and negative if $f > n$. By reversing the indices we change the sign

$$\Delta A_{j,k} = -\Delta A_{k,j} \quad (12)$$

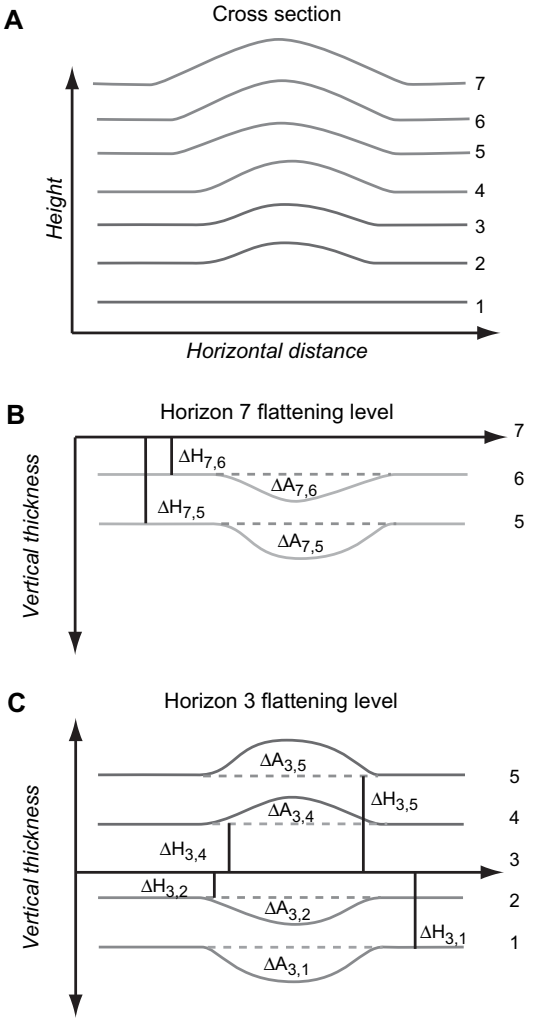

Fig. 14. Schematic example of measurement of thickness relief and height with multiple flattening horizons, as discussed in Appendix A.

Similarly

$$\Delta H_{j,k} = -\Delta H_{k,j} \tag{13}$$

For example $\Delta A_{3,5}$ is the thickness relief of horizon 5 relative to a flattening level 3 and is equal in magnitude and opposite in sign to $\Delta A_{5,3}$, which is the thickness relief of horizon 3 relative to a flattening level 5 (Fig. 14).

We use a simple example shown in Fig. 14 composed of seven horizons to illustrate the basic application of Eqs. (9)–(13) to obtain the areas and heights. Our goal is to get the areas of structural relief and heights with respect to horizon 1, which is the detachment level. We choose two horizons for flattening. Horizon 7 at the top of the pregrowth section is chosen because flattening at this level will show the stratigraphic architecture just prior to deformation and because it is the most distorted horizon. We obtain measurements of thickness relief and height for horizons 5 and 6 relative to level 7, which are negative quantities. Horizon 3 in the middle of the section is also chosen for flattening, yielding measurements for horizons 1, 2, 4 and 5. Since horizon 5 is common to the two data sets we can compute the areas of structural relief and heights for each horizon relative to detachment level 1 from the primary thickness-relief measurements. For example

$$A_{1,2} = \Delta A_{1,2} = \Delta A_{1,3} + \Delta A_{3,2} = -\Delta A_{3,1} + \Delta A_{3,2}$$

and

$$H_{1,2} = \Delta H_{1,2} = \Delta H_{1,3} + \Delta H_{3,2} = -\Delta H_{3,1} + \Delta H_{3,2}$$

where $(\Delta A_{3,1}, \Delta H_{3,1})$ and $(\Delta A_{3,2}, \Delta H_{3,2})$ are the primary measurements. The entire set of areas of structural relief, written in terms of the primary thickness-relief measurements, is

$$A_{1,2} = \Delta A_{1,2} = \Delta A_{1,3} + \Delta A_{3,2} = -\Delta A_{3,1} + \Delta A_{3,2}$$

$$A_{1,3} = \Delta A_{1,3} = -\Delta A_{3,1}$$

$$A_{1,4} = \Delta A_{1,3} + \Delta A_{3,4} = -\Delta A_{3,1} + \Delta A_{3,4}$$

$$A_{1,5} = \Delta A_{1,3} + \Delta A_{3,5} = -\Delta A_{3,1} + \Delta A_{3,5}$$

$$\begin{aligned} A_{1,6} &= \Delta A_{1,3} + \Delta A_{3,5} + \Delta A_{5,6} \\ &= -\Delta A_{3,1} + \Delta A_{3,5} - \Delta A_{7,5} + \Delta A_{7,6} \end{aligned}$$

$$A_{1,7} = \Delta A_{1,3} + \Delta A_{3,5} + \Delta A_{5,7} = -\Delta A_{3,1} + \Delta A_{3,5} - \Delta A_{7,5}$$

The computation for height is analogous.

Appendix B. Determination of regional stratigraphic gradient in the depth domain from thickness relief

In order to measure the curvimetric shortening $S_c = (L_d - L)$ we must determine the undeformed regional stratigraphic gradient so that we can measure the bed length L (Fig. 1). We determine the undeformed regional gradient from the same data that we used in the thickness-relief analysis. The key intermediate step in this analysis is the determination of the total relief R_{n,x_i} between the present deformed shape of a horizon n and its undeformed regional gradient at each discrete horizontal position x_i, as shown in Fig. 15a. Once we determine the set of all $\langle x_i, R_{n,x_i}\rangle$ we can calculate the shape of the undeformed regional gradient $\langle x_i, (z_{n,x_i} - R_{n,x_i})\rangle$ given the deformed shape of the horizon $\langle x_i, z_{n,x_i}\rangle$. We can then use these results to compute the deformed L_d and undeformed L bed length and the curvimetric shortening $S_c = (L_d - L)$.

The total relief R_{n,x_i} between a deformed horizon and its undeformed regional gradient is simply the sum of the differences in relief $\Delta R_{k,k+1,x_i}$ between all the intervening adjacent horizons k and $k+1$ between the horizon in question n and some undeformed reference surface r

$$\begin{aligned} R_{r,n,x_i} &= \Delta R_{r,r+1,x_i} + \Delta R_{r+1,r+2,x_i} + \cdots + \Delta R_{n,n-1,x_i} \\ &= \sum_{k=r}^{n-1} \Delta R_{k,k+1,x_i} \end{aligned} \tag{14}$$

In practice we measure the quantities $\Delta R_{f,n,x_i}$ in the thickness domain as part of the process of computing the local area of thickness relief, relative to some flattening horizon f. As before with thickness relief, if $f < n$ then $\Delta R_{f,n,x_i} > 0$ in compression (pregrowth strata), therefore if we reverse the indices we change the sign

$$\Delta R_{j,k,x_i} = -\Delta R_{k,j,x_i} \tag{15}$$

For example $\Delta R_{3,5,x_i}$ is the contribution of relief of horizon 5 relative to flattening level 3 and is equal in magnitude and opposite in sign to $\Delta R_{5,3,x_i}$, which is the contribution of relief of horizon 3 relative to flattening level 5.

There are errors associated with each local relief measurement gradient $\Delta R_{f,n,x_i}$ that in practice makes the computed undeformed regional gradient $\langle x_i, (z_{n,x_i} - R_{n,x_i})\rangle$ noisy relative to the present deformed shape of the horizon. Therefore, $\langle x_i, R_{n,x_i}\rangle$ must be smoothed to the point that its noise is similar to the noise of the present deformed shape of the horizon $\langle x_i, z_{n,x_i}\rangle$. Then the deformed L_d and undeformed L bed length and the curvimetric shortening $S_c = (L_d - L)$ can be computed.

We use the same simple example composed of seven horizons that we used in Appendix A (Fig. 14) to illustrate the basic application of Eqs. (14) and (15) to determine the regional gradient for computing curvimetric shortening S_c, based on our previous measurements in the thickness domain as shown in Fig. 15. As part of our determination of the area of the thickness relief we make measurements of local relief $\Delta R_{f,n,x_i}$ between each horizon n and flattening horizons f (7 and 5) at a set of regularly spaced horizontal locations x_i. This set of measurements $\langle x_i, R_{n,x_i}\rangle$ is used to compute the area of thickness relief $\Delta A_{f,n}$. We obtain measurements of local relief for horizons 5 and 6 relative to flattening level 7, which are negative quantities. Horizon 3 in the middle of the section is also chosen for flattening, yielding

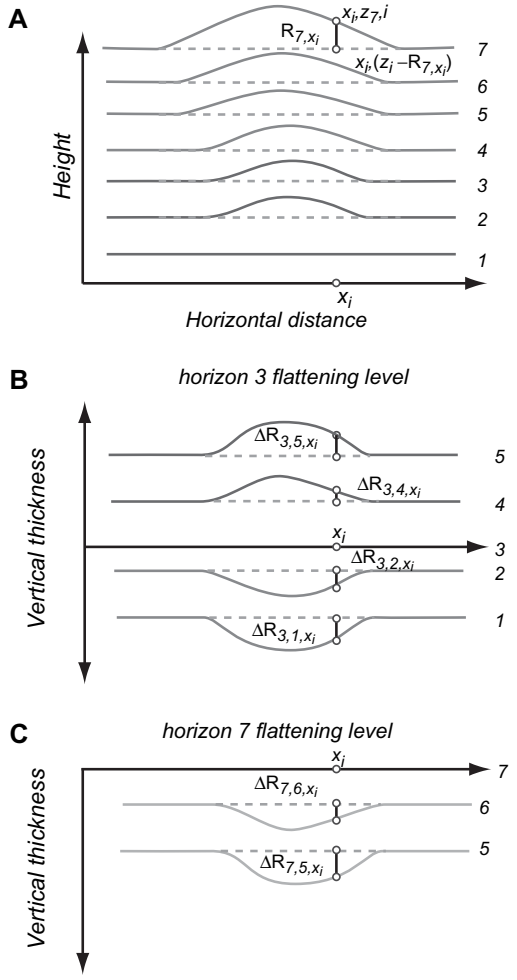

Fig. 15. Schematic example of determination of deformed regionals in depth from measurements of flattened horizons, which is a key step in determining curvimetric shortening, as discussed in Appendix B.

measurements for horizons 1, 2, 4 and 5. Since horizon 5 is common to the two data sets we can compute the total relief $\langle R_{n,x_i} \rangle$ for each horizon and horizontal position. For example

$$R_{2,x_i} = \Delta R_{1,2,x_i} = \Delta R_{1,3,x_i} + \Delta R_{3,2,x_i} = -\Delta R_{3,1,x_i} + \Delta R_{3,2,x_i}$$

where $\Delta R_{3,1,x_i}$ and $\Delta R_{3,2,x_i}$ are the primary relief measurements. The entire set of total relief measurements at a single horizontal position x_i, written in terms of the primary thickness-relief measurements, is

$$R_{2,x_i} = \Delta R_{1,2,x_i} = \Delta R_{1,3,x_i} + \Delta R_{3,2,x_i} = -\Delta R_{3,1,x_i} + \Delta R_{3,2,x_i}$$

$$R_{3,x_i} = \Delta R_{1,3,x_i} = -\Delta R_{3,1,x_i}$$

$$R_{4,x_i} = \Delta R_{1,3,x_i} + \Delta R_{3,4,x_i} = -\Delta R_{3,1,x_i} + \Delta R_{3,4,x_i}$$

$$R_{5,x_i} = \Delta R_{1,3,x_i} + \Delta R_{3,5,x_i} = -\Delta R_{3,1,x_i} + \Delta R_{3,5,x_i}$$

$$R_{6,x_i} = \Delta R_{1,3,x_i} + \Delta R_{3,5,x_i} + \Delta R_{5,6,x_i} = -\Delta R_{3,1,x_i} + \Delta R_{3,5,x_i} - \Delta R_{7,5,x_i} + \Delta R_{7,6,x_i}$$

$$R_{7,x_i} = \Delta R_{1,3,x_i} + \Delta R_{3,5,x_i} + \Delta R_{5,7,x_i} = -\Delta R_{3,1,x_i} + \Delta R_{3,5,x_i} - \Delta R_{7,5,x_i}$$

We can now compute the shape of the regional stratigraphic gradient in the depth domain for each horizon, which is $\langle x_i, (z_{n,x_i} - R_{n,x_i}) \rangle$. For example for horizon 7, as shown in Fig. 15a, the elevation of the undeformed regional is $(z_{7,x_i} - R_{7,x_i})$, where z_{7,x_i} is the elevation of the deformed horizon at the same horizontal position x_i. After smoothing the noise in the regional stratigraphic gradient we can compute the bed lengths and curvimetric shortening.

References

Adam, J., Klaeschen, D., Kukowski, N., Flueh, E., 2004. Upward delamination of Cascadia Basin sediment infill with landward frontal accretion thrusting caused by rapid glacial age material flux. Tectonics 23, TC3009.

Atkinson, P.K., Wallace, W.K., 2003. Competent unit thickness variation in detachment folds in the Northeastern Brooks Range, Alaska: geometric analysis and a conceptual model. Journal of Structural Geology 25, 1751–1771.

Bangs, N.L.B., Gulick, S.P.S., 2005. In: Mikada, H., Moore, G.F., Taira, A., et al. (Eds.), Physical properties along the developing décollement in the Nankai Trough: inferences from 3-D seismic reflection data inversion and Leg 190 and 196 drilling data. Proceedings of the Ocean Drilling Program, Scientific Results 190/196. Available from: http://www-odp.tamu.edu/publications/190196SR/354/354.htm (accessed 16.11.05.).

Bilotti, F., Shaw, J., 2005. Deep-water Niger Delta fold and thrust belt modeled as a critical-taper wedge: the influence of elevated basal fluid pressure on structural styles. American Association of Petroleum Geologists Bulletin 89, 1475–1491.

Bilotti, F., Shaw, J., Cupich, R., Lakings, R., 2005. Detachment fold, Niger Delta. In: Shaw, J., Connors, C., Suppe, J. (Eds.), Seismic Interpretation of Contractional Fault-Related Folds. American Association of Petroleum Geologists, Tulsa, 156 pp.

Bucher, W.H., 1933. The Deformation of the Earth's Crust; An Inductive Approach to the Problems of Diastrophism. Princeton University Press, Princeton.

Bulnes, M., Poblet, J., 1999. Estimating the detachment depth in cross sections involving detachment folds. Geological Magazine 136, 395–412.

Carson, B., Westbrook, G.K., Musgrave, R.J., et al. (Eds.), 1995. Proceedings of the Ocean Drilling Program, Scientific Results 146 Part 1, Ocean Drilling Program.

Chamberlain, R.T., 1910. The Appalachian folds of central Pennsylvania. Journal of Geology 18, 228–251.

Chamberlain, R.T., 1919. The building of the Colorado Rockies. Journal of Geology 27, 145–164.

Cochrane, G.R., Moore, J.C., Mackay, M.E., Moore, G.F., 1994. Velocity and inferred porosity model of the Oregon accretionary prism from multichannel seismic reflection data: implication on sediment dewatering and overpressure. Journal of Geophysical Research 99, 7033–7043.

Cohen, H.A., McClay, K.R., 1996. Sedimentation and shale tectonics of the northwestern Niger Delta front. Marine and Petroleum Geology 13, 313–328.

Corredor, F., Shaw, J., Bilotti, F., 2005a. Structural styles in the deep-water fold and thrust belts of the Niger Delta. American Association of Petroleum Geologists Bulletin 89, 753–780.

Corredor, F., Shaw, J., Suppe, J., 2005b. Shear fault-bend folding, deep water Niger delta. In: Shaw, J., Connors, C., Suppe, J. (Eds.), Seismic Interpretation of Contractional Fault-Related Folds, American Association of Petroleum Geologists, Tulsa, 87–92.

Dahlstrom, C.D.A., 1990. Geometric constraints derived from the law of conservation of volume and applied to evolutionary models for detachment folding. American Association of Petroleum Geologists Bulletin 74, 336–344.

Epard, J.L., Groshong, J.R.H., 1993. Excess area and depth to detachment. American Association of Petroleum Geologists Bulletin 77, 1291–1302.

Epard, J.L., Groshong, J.R.H., 1995. Kinematic model of detachment folding including limb rotation, fixed hinges and layer-parallel strain. Tectonophysics 247, 85–103.

Erslev, E.A., Mayborn, K.R., 1997. Multiple geometries and modes of fault-propagation folding in the Canadian thrust belt. Journal of Structural Geology 19, 321–335.

Freund, J.E., 1997. Modern Elementary Statistics. Prentice Hall, Upper Saddle River, NJ.

Goguel, J., 1962. Tectonics. W.H. Freeman, San Francisco.

Gonzalez-Mieres, R., Suppe, J. Shortening histories in active detachment folds. In: McClay, K.R., Shaw, J., Suppe, J. (Eds.), Thrust Fault-Related Folding. American Association of Petroleum Geologists, Tulsa, submitted for publication.

Grimes, D., Gringer, E., Spokes, J., 2004. Agbami field Nigeria – addressing challenges and uncertainty. Houston Geological Society Bulletin 46, 19–21.

Groshong, J.R.H., 1994. Area balance, depth to detachment, and strain in extension. Tectonics 13, 1488–1497.

Groshong, J.R.H., 1996. Construction and validation of extensional cross sections using lost area and strain, with application to the Rhine Graben. In: Buchanan, P.G., Nieuwland, D.A. (Eds.), Modern Developments in Structural Interpretation, Validation and Modeling. Geological Society, London, Special Publication 99, 79–87.

Groshong, J.R.H., Epard, J.L., 1994. The role of strain in area-constant detachment folding. Journal of Structural Geology 16, 613–618.

Gulick, S.S., Bangs, N.L., Shipley, T.H., Nakamura, Y., Moore, G.F., Kuramoto, S., 2004. Three-dimensional architecture of the Nankai accretionary prism's imbricate thrust zone off Cape Muroto, Japan: prism reconstruction via en echelon thrust propagation. Journal of Geophysical Research 109, doi:10.1029/2003JB002654.

Hamilton, E., 1978. Sound velocity–density relations in sea-floor sediments and rocks. Journal of the Acoustical Society of America 63, 366–377.

Henry, P., Jouniaux, L., Screaton, E.J., Hunze, S., Saffer, D.M., 2003. Anisotropy of electrical conductivity record of initial strain at the toe of the Nankai accretionary wedge. Journal of Geophysical Research 108, 2407, doi:10.1029/2002JB002287.

Higuera-Díaz, I.C., Fischer, M.P., Wilkerson, M.S., 2005. Geometry and kinematics of the Nuncios detachment fold complex: implications for lithotectonics in northeastern Mexico. Tectonics 24, TC4010.

Homza, T.X., Wallace, W.K., 1995. Geometric and kinematic models for detachment folds with fixed and variable detachment depths. Journal of Structural Geology 17, 575–588.

Homza, T.X., Wallace, W.K., 1997. Detachment folds with fixed hinges and variable detachment depth, northeastern Brooks Range, Alaska. Journal of Structural Geology 19, 337–354.

Hooper, R.J., Fitzsimmons, R.J., Grant, N., Vendeville, B.C., 2002. The role of deformation in controlling depositional patterns in the south-central Niger Delta, West Africa. Journal of Structural Geology 24, 847–859.

Hubert-Ferrari, A., Suppe, J., Wang, X., Jia, C., 2005. The Yakeng detachment fold, South Tianshan, China. In: Shaw, J., Connors, C., Suppe, J. (Eds.), Seismic Interpretation of Contractional Fault-Related Folds. American Association of Petroleum Geologists, Tulsa, 110–113.

Hubert-Ferrari, A., Suppe, J., Gonzalez-Mieres, R., Wang, X. Active folding of the landscape in the southern Tianshan, China. Journal of Geophysical Research, in press.

Jamison, W.R., 1987. Geometric analysis of fold development in overthrust terranes. Journal of Structural Geology 9, 207–219.

Karig, D.E., Angevine, C.L., 1986. In: Kagami, H., Karig, D.E., Bray, C.J., et al. (Eds.), Geologic Constraints on Subduction Rates in the Nankai Trough. Initial Reports of the Deep Sea Drilling Project 87, 789–796.

Kulm, L.D., Louhere, P.W., Peper, J.S. (Eds.), 1984. Western North American Continental Margin and Adjacent Ocean Floor off Oregon and Washington. Marine Science International, Woods Hole.

Laubscher, H.P., 1961. Die Fernschubhypothese der Jurafaltung. Eclogae Geologicae Helvetiae 54, 221–282.

Laubscher, H.P., 1965. Ein kinematisches Theorie der Jurafaltung. Eclogae Geologicae Helvetiae 58, 231–318.

Laubscher, H.P., 1966. Zur Kinematik und Dynamik des noerdlichen Rheintalischen Juras. Eclogae Geologicae Helvetiae 59, 957–959.

Le Pichon, X., Iiyama, T., Chamley, H., Charvet, J., Faure, M., Fujimoto, H., Furuta, T., Ida, Y., Kagami, H., Lallemant, S., 1987. Nankai Trough and the fossil Shikoku Ridge: results of Box 6 Kaiko survey. Earth and Planetary Science Letters 83, 186–198.

MacKay, M.E., 1995. Structural variation and landward vergence at the toe of the Oregon accretionary prism. Tectonics 14, 1309–1320.

MacKay, M.E., Moore, G.F., Cochrane, G.R., Moore, C.J., Kulm, L.D., 1992. Landward vergence and oblique structural trends in the Oregon margin accretionary prism: implications and effect on fluid flow. Earth and Planetary Science Letters 109, 477–491.

Masaferro, J., Poblet, J., Bulnes, M., Eberli, G.P., Dixon, T., McClay, K.R., 1999. Palaeogene–Neogene/present day growth folding in the Bahamian foreland of the Cuban fold and thrust belt. Journal of the Geological Society 156, 617–631.

Mitra, S., Namson, J., 1989. Equal-area balancing. American Journal of Science 289, 563–599.

Miyazaki, S., Heki, K., 2001. Crustal velocity field of southwest Japan: subduction and arc–arc collision. Journal of Geophysical Research 106, 4305–4326.

Moore, G.F., Karig, D., Shipley, T.H., Taira, A., Stoffa, P.L., Wood, W.T., 1991. Structural framework of the ODP Leg 131 area, Nankai Trough. In: Taira, A., Hill, I.A., Firth, J.V., et al. (Eds.), Proceedings of the Ocean Drilling Program, Initial Reports 131. Ocean Drilling Project, College Station, TX, pp. 15–20.

Moore, G.F., Shipley, T.H., Stoffa, P.L., Karig, D.E., Taira, A., Kuramoto, S., Tokuyama, H., Suyehiro, K., 1990. Structure of the Nankai Trough accretionary zone from multichannel seismic reflection data. Journal of Geophysical Research 95, 8753–8765.

Moore, G.F., Taira, A., Bangs, N.L., et al., 2001a. Data report: structural setting of the Leg 190 Muroto Transect. In: Moore, G.F., Taira, A., Klaus, A., et al. (Eds.), Proceedings of the Ocean Drilling Program, Initial Reports 190, 1–14. Available from: http://www-odp.tamu.edu/publications/190_IR/VOLUME/CHAPTERS/IR190_02.PDF.

Moore, G.F., Taira, A., et al., 2001b. New insights into deformation and fluid flow processes in the Nankai Trough accretionary prism: results of Ocean Drilling Program Leg 190. Geochemistry, Geophysics, Geosystems 2. 2001GC000166.

Moore, J.C., Moran, K., MacKay, M.E., Tobin, H., 1995. Frontal thrust, Oregon accretionary prism: geometry, physical properties, and fluid pressure. In: Carson, B., Westbrook, G.K., Musgrave, R.J., Suess, E. (Eds.), Proceedings of the Ocean Drilling Program, Scientific Results, 146 (Pt. 1). Ocean Drilling Program, College Station, TX, 359–366.

Mugnier, J.L., Vialon, P., 1986. Deformation and displacement of the Jura cover on its basement. Journal of Structural Geology 8, 373–387.

Pashin, J.C., Groshong, J.R.H., Wang, S., 1995. Thin-skinned structures influence gas and water production in Alabama coalbed methane fields. In: Intergas '95, International Unconventional Gas Symposium, 39–52.

Poblet, J., Hardy, S., 1995. Reverse modeling of detachment folds; application to the Pico del Águila anticline in the South Central Pyrenees (Spain). Journal of Structural Geology 17, 1707–1724.

Poblet, J., McClay, K.R., 1996. Geometry and kinematics of single-layer detachment folds. American Association of Petroleum Geologists Bulletin 80, 1085–1109.

Rico, L., 1999. Geometric and Kinematic Evolution of a Complete Detachment Fold in a Natural Cross-Section. Unpublished M.S. thesis, University of Texas, Austin.

Rowan, M.G., 1997. Three-dimensional geometry and evolution of a segmented detachment fold, Mississippi fan foldbelt, Gulf of Mexico. Journal of Structural Geology 19, 463–480.

Rowan, M.G., Kligfield, R., Weimer, P., 1993. Processes and rates of deformation: preliminary results from the Mississippi fan foldbelt, deep Gulf of Mexico. In: GCSSEPM Foundation 14th Annual Research Conference, Programs with Papers, 209–218.

Seno, T., 1977. The instantaneous rotation vector of the Philippine Sea plate relative to the Eurasian plate. Tectonophysics 42, 209–226.

Serra, O., 1984. Fundamentals of Well-Log Interpretation. Elsevier & Elf Aquitaine, Amsterdam.

Shaw, J., Connors, C., Suppe, J., 2005. Part 1: Structural interpretation methods. In: Shaw, J., Connors, C., Suppe, J. (Eds.), Seismic Interpretation of Contractional Fault-Related Folds. American Association of Petroleum Geologists, Tulsa, 1–58.

Shipboard-Scientific-Party, 2001a. Leg 190 summary. In: Moore, G.F., Taira, A., Klaus, A., et al. (Eds.), Proceedings of the Ocean Drilling Program, Initial Reports, 190, 1–87. Available from: http://www-odp.tamu.edu/publications/190_IR/VOLUME/CHAPTERS/IR190_01.PDF.

Shipboard-Scientific-Party, 2001b. Site 1174. In: Moore, G.F., Taira, A., Klaus, A., et al. (Eds.), Proceedings of the Ocean Drilling Program, Initial Reports, 190, 1–149. Available from: http://www-odp.tamu.edu/publications/190_IR/VOLUME/CHAPTERS/IR190_05.PDF.

Silver, E.A., 1972. Pleistocene tectonic accretion of the continental slope off Washington. Marine Geology 13, 239–249.

Suppe, J. Mass balance and thrusting in detachment folds. In: McClay, K.R., Shaw, J., Suppe, J. (Eds.), Thrust Fault-Related Folding. American Association of Petroleum Geologists, Tulsa, submitted for publication.

Suppe, J., Connors, C.D., Zhang, Y., 2004. Shear fault-bend folding. In: McClay, K.R. (Ed.), Thrust Tectonics and Hydrocarbon Systems, Memoir 82. American Association of Petroleum Geologists, Tulsa, 303–323.

Taira, A., Hill, I., Firth, J., Berner, U., Bruckmann, W., Byrne, T., Chabernaud, T., Fisher, A., Foucher, J.-P., Gamo, T., 1992. Sediment deformation and hydrogeology of the Nankai Trough accretionary prism: synthesis of shipboard results of ODP Leg 131. Earth and Planetary Science Letters 109, 431–450.

Weimer, R.C., 1987. Applied Elementary Statistics. Brooks/Cole Pub. Co., Monterey, Calif.

Westbrook, G.K., Carson, B., Musgrave, R.J., et al., 1994. Leg 146 introduction; Cascadia margin. In: Westbrook, G.K., Carson, B., Musgrave, R.J., et al. (Eds.), Proceedings of the ODP, Initial Report 146. Ocean Drilling Program, College Station TX, 5–14.

Wiltschko, D.V., Chapple, M.V., 1977. Flow of weak rocks in Appalachian Plateau folds. American Association of Petroleum Geologists Bulletin 61, 653–670.